Aalto University
School of Engineering

Miikka Pennanen

OPTIMAL SAILOR POSITION ON AN OLYMPIC DINGHY

Master's Thesis submitted in partial fulfilment of the requirements for degree of Master of Science in Technology.

Helsinki, 9 November 2015

Supervisor: Professor Jani Romanoff, Aalto University

Instructor: Professor Lars Larsson, Chalmers University

Aalto University
School of Engineering

Aalto University, P.O. BOX 11000, 00076
AALTO
www.aalto.fi

Abstract of master's thesis

Author	Miikka Pennanen
Title of thesis	Optimal Sailor Position on an Olympic Dinghy
Degree programme	Department of Applied Mechanics
Major/minor	Marine Technology
Code	K3005
Thesis supervisor	Professor Jani Romanoff
Thesis advisor(s)	Professor Lars Larsson
Date	09.11.2015
Number of pages	56
Language	Englanti

Abstract

As the Laser Olympic dinghy is one of the highest level sail racing classes in the world, there is an interest in obtaining scientific facts around the tons of experience that already exist. For this reason, a numerical investigation was carried out to find the optimum heel and trim angles for upwind sailing. Flat water was assumed.

Systematic Computational Fluid Dynamics (CFD) Simulations were carried out to find the optimum trim versus heel at speeds of two, three, four and five knots. During these computations the leeway was fixed for each speed. The leeway angles were estimated using the resistance results obtained from the tank tests and foil theory. A special purpose VPP was developed accepting CFD results at the given speeds as input for the hydrodynamic forces, while the aerodynamic forces were obtained using Hazen's empirical model. The output from the program was the true wind speed required to achieve the target speed at 45 degrees true wind angle. By systematic variation of the sailor's position the optimum heel (and the corresponding trim) was obtained at the minimum required wind speed.

The reason for developing this unconventional VPP was to avoid interpolation between the speeds computed by CFD. Since the resistance/speed relation is very non-linear interpolation would have been too approximate for finding the rather flat heel/trim optima.

The computational techniques and the optimum heel and trim angles of the dinghy will be reported in this thesis. In the course of the computations several interesting flow phenomena were investigated, such as the interactions between the centreboard and the rudder, and between the hull and the appendages. These by-products will be briefly reported in the Conclusions and Future Work –chapter.

Keywords VPP, Sailing, CFD, Hydrodynamics

Aalto University
School of Engineering

Aalto University, P.O. BOX 11000, 00076
AALTO
www.aalto.fi

Abstract of master's thesis

Tekijä Miikka Pennanen		
Työn nimi Purjehtijan Optimaalinen Positio Olympialuokan Jollassa		
Koulutusohjelma Sovelletun mekaniikan laitos		
Pää-/sivuaine Meritekniikka		**Koodi** K3005
Työn valvoja Professori Jani Romanoff		
Työn ohjaaja(t) Professori Lars Larsson		
Päivämäärä 09.11.2015	**Sivumäärä** 56	**Kieli** Englanti

Tiivistelmä

Olympiajolla Laser on maailman kovatasoisimpia ja kilpailluimpia purjehdusluokkia, joten on kiinnostavaa etsiä tieteellisiä faktoja olemassa olevan laajan käytännön kokemuksen ympärille. Tällaisen tieteellisen faktan tuottamiseksi tässä tutkimuksessa on ratkaistu Laser-jollan optimaaliset kallistus- ja viippauskulmat laskennallisesti. Tutkimus koskee vastatuulipurjehdusta ja olettaa aallottoman vedenpinnan.

Optimaalisen kulkuasennon löytämiseksi suoritettiin systemaattinen sarja virtaussimulointeja (CFD) kahden, kolmen, neljän ja viiden solmun nopeuksissa. Näissä simuloinneissa sortokulma oli määrittetty vakioksi jokaiselle nopeudelle erikseen. Sortokulmat arvioitiin käyttämällä allaskokeiden tuloksia sekä laskemalla evien tuottama vastus ja sivuttainen voima analyyttisesti. Erityinen purjeveneen suorituskykyä arvioiva ohjelma (VPP) kehitettiin tämän tutkimuksen sisällä. Ohjelman hydrodynaamisina lähtöarvoina käytettiin CFD tuloksia määrätylle nopeudelle. Aerodynaamiset voimat ratkaistiin Hazenin empiirisestä purjeaerodynamiikka -mallista. Ohjelman tuloksena saatiin tarvittava tuulen nopeus, jotta vene purjehtii 45 asteen kulmassa tuuleen määrätyllä nopeudella. Muuttamalla veneen kulkuasentoa systemaattisesti löydettiin veneen optimaalinen kulkuasento kallistuksen ja viippauksen suhteen pisteestä, jossa vene tarvitsi vähiten tuulta saavuttaakseen määrätyn nopeuden.

Erityinen käänteinen VPP kehitettiin, jotta pystyttiin välttämään interpolointi CFD-simuloinneissa ratkaistujen nopeuksien välillä. Vastuskäyrän epälineaarisuudesta johtuen nopeuksien välinen interpolointi olisi vähentänyt tutkimuksen tarkkuutta.

Tutkimuksessa käytetyt laskennalliset tekniikat ja optimaaliset kallistuskulmien tulokset esitetään tässä tutkimuksessa. Simulointien yhteydessä tutkittiin monia mielenkiintoisia virtausilmiöitä, kuten kölin ja peräsimen välistä vuorovaikutusta ja vastaavasti rungon ja kölin vuorovaikutusta. Näitä sivuhavaintoja käsitellään lyhyesti työn lopussa.

Avainsanat VPP, Purjehdus, CFD, Hydrodynamiikka

PREFACE

This thesis has been written as co-operative project of Aalto University Department of Applied Mechanics and Chalmers University Department of Shipping and Marine Technology. The work was mainly carried out at Chalmers University in Gothenburg.

This thesis is part of the research within the field of sailing dynamics at Chalmers University. It has been instructed by Professor Lars Larsson and PhD student Rickard Lindstrand Levin. Professor Jani Romanoff from Aalto University has supervised the thesis. The aim is to find the optimal sailor position on an Olympic dinghy in upwind conditions in flat water. Funding of the thesis has been supported by Aalto University and Merenkulun säätiö (Maritime foundation in Finland).

I am grateful for the seamless co-operation between the Universities and all the positive attitudes towards the exchange. Also I am thankful for the financial support from Aalto University and Merenkulun säätiö. During my thesis professor Jani Romanoff has provided remarkably clear and structured supervision, professor Lars Larsson has generously shared his knowledge, experience and passion on a daily basis, and PhD student Rickard Lindstrand Levin has guided me through the large amount of simulations. It has been a great team to work with! Thank you!

Driven by my passion towards sailing yachts I have studied Naval Architecture in three different universities in Helsinki, Southampton and Gothenburg. The different experiences have had an invaluable impact on my professional knowledge as well as many friendships all over the planet. I want to thank my professor Jerzy Matusiak and researcher Tommi Mikkola for recognizing my interests and supporting them. I also want to thank my parents Pirjo and Risto Pennanen and my wife Silja Kanerva for all the encouragement and for making my choices possible.

Helsinki, 9 November 2015

Miikka Pennanen

TABLE OF CONTENTS

LIST OF SYMBOLS

Notations

A	Area
A_e	Effective aspect ratio
AR	Aspect ratio
$AR\ laser$	Aspect ratio as modified for Laser
$Asail$	Sail area
BAD	Boom above deck
c	Chord length
C_d	Drag coefficient
Cd_i	Induced drag coefficient
CE	Centre of effort
Cf	Friction coefficient
Cl	Lift coefficient
C_m	Mean chord
D	Drag
D_i	Induced drag
E	Foot length of the sail
EHM	Mast height above the sheerline
FA	Average freeboard height
L	Characteristic length
$Lsail$	Lift of the sail
$M_{Heeling}$	Heeling Moment
t	thickness of wing section
V	Velocity
V_{AW}	Apparent wind velocity

P	Luff length of the sail
R_f	Frictional resistance
RM_{max}	Maximum righting moment
Rn	Reynolds number
R_{tot}	Total resistance
S	Planform area
Sw	Wetted surface area
Y+	Dimensionless wall distance
(1+k)	Hoerner form factor
μ	Dynamic viscosity
ρ	density
v	Kinematic viscosity

Abreviations

CB	Centre of buoyancy
CFD	Computational fluid dynamics
CLR	Centre of lateral resistance
COG	Centre of Gravity
CPU	Central processing unit
CSYS	Chesapeake Sailing Yacht Symposium
DNS	Direct numerical simulation
GZ	Righting arm
HPYD	High Performance Yacht Design Conference
IDF	Induced drag factor
ITTC	International towing tank conference
IVPP	Inverse Velocity Prediction Program
kn	knots
Laser	The single handed Olympic sailing dinghy Laser
LES	Large eddy simulation
RANS	Reynolds-averaged Navier-Stokes
SF	Side force
VOF	Volume of fluid
VPP	Velocity Prediction Program

1 Introduction

1.1 Context

Sport is a common interest for almost all people, regardless of level of education or other background. Therefore sport has been found to be a very inspiring field for technological development, giving a common and passionate interdisciplinary platform for studies and research for a variety of people from different backgrounds. At Chalmers University this has inspirational topic has been used for research and student projects with good success. A specific Sports and Technology program is run by the Material Technology department and focuses on sailing, horse racing and swimming.

Research within sailing is currently carried out in many universities and companies all over the world. Probably the most significant conferences to gather and promote scientific research in the field at the moment are the High Performance Yacht Design conference (HPYD) in New Zealand, the Chesapeake Sailing Yacht Symposium (CSYS) held in the United States and Innovsail organized in France. Each of these is held tri-annually. Chalmers University has actively participated presenting papers especially at HPYD.

1.2 Background

During the past 20 years sport has developed into a full time profession. The level in professional sports is very high and the top athletes have the possibility to fully concentrate on their sport. As sports is becoming more serious and in some sense comparable to other jobs or industries, research and development is done in in the field as in any other business. Improving equipment within the class rules is common practice similarly to a research and development project in some other industry. Also gaining the understanding of sailors and improving their techniques through a research project is common. This thesis is such a project as the Laser is a strict one design class and no changes on the equipment can be made.

In addition to the sport itself also technology is constantly and rapidly developing. Many types of technical equipment suitable for research have become easily available and is utilised by sportsmen, their coaches and support teams. A common example of such equipment would be a high resolution camera. A slightly less accessible example would be a motion tracking system. A very high-end example would be a computer cluster capable of solving Computational Fluid Dynamics (CFD) -simulations coupled with optimization algorithms.

1.3 Previous work within Chalmers Sailing Dynamics

Research within sailing has been carried out at Chalmers University for a very long time. Professor Lars Larsson has been guiding this work with great passion and many of his students have done master´s theses within sailing related topics. Recent theses carried out have among others investigated sailing yacht fore body shapes (Pluto et al. 2015), Sailing yacht transom shapes (Alroth et al. 2014), and bulb keel shapes (Axfors et al. 2011, Ljungqvist 2011). Several papers have also been published based on the theses.

Also Chalmers University has had two doctoral students within sailing. Rickard Lindstrand Levin is currently working within research on sailing dynamics on the Laser dinghy and Sofia Werner completed her doctoral thesis on bulb winglets in 2006 (Werner 2006).

1.4 State of the Art

The correct prediction of resistance and power is an essential problem in ship and boat design, as the designed vessel always has some type of target speed. This target speed might be defined in many different ways. On commercial vessels the target is normally a certain speed that has to be achieved with specific power consumption (Larsson et al. 2010). On a racing sailing yacht the target speed could be defined as the average velocity made good around a race course having to be higher than the same for any competitor.

Essentially the problem on a container ship or on a racing sailing yacht is the same, being the balance of resistance and propulsion. However, the applied flow phenomena of propeller and sail propulsion or a heavy displacement ship and a light catamaran hull differ quite a bit. Still, they are based on the very same principles.

In the following chapters the state of the art within the relevant areas for this study will briefly be presented. It is the balance of sailing forces that is studied in this thesis and the relevant areas to this are prediction of resistance, velocity prediction programs (VPP) and computational fluid dynamics.

1.4.1 Prediction of Resistance

There are three main methods of predicting resistance which are model testing, using empirical methods and computational techniques. All of these methods are today widely in use in most areas of marine design (Larsson 2010). While model testing of ships is an old method that has been stated to first have been used by Leonardo Da Vinci in the 15th century (Tursini 1953), it has remained in very key position when testing new concepts and validating computational results. Naturally the methods have been greatly improved since DaVinci´s time and the accuracy of model tests is commonly regarded to be within small margins of error (Molland 2008, p. 217). The current methods used in

international towing tanks are generally based on the ITTC-78 procedure that has last been modified in 1984 (ITTC 2000), therefore model tests on ship resistance have changed very little during recent years. A large portion of the science within model testing concentrates on how the resistance components are scaled. In this study this is not a relevant question, as the tank tests were performed in full scale.

With the advent of powerful computers, computational fluid dynamics simulation has become a significant tool in ship and yacht design. As simulations can be performed both in model and full scale, simulations have also provided a comparison to the scaling methods used within physical model testing. Many of the scaling methods used within tank testing have been questioned and it is often argued whether a full scale CFD result is more accurate than a scaled model test. This, off course is case dependent, but generally CFD simulations have challenged the old tank testing methods and pushed their development (Stern et al. 2012).

Within model tests of sailing yachts the same procedures as in the ship industry are used, but some important factors to sailing yachts, like the side force need a refined measurement arrangement. There are two different main approaches to sailing yacht towing tank testing. The first method is the so called free method, where the yacht is towed from a mast like post from the estimate centre of effort of the sails. The yacht then runs freely and is balanced by its rudder. In this way every run in the tank represents a real sailing condition. The models in this kind of towing tank test are demanding to produce as stability properties have to be correct in model scale compared to full scale. This also makes changes of stability during the design process troublesome (Fossati 2007, Larsson 2014).

The other approach is the so called semi-captive method where the movement of the model is restricted in all other directions than pitch and heave. Several runs are made over a variety of leeway and heel angles. By balancing the aerodynamic forces analytically to the tested hydrodynamic forces the sailing equilibrium is found. This approach is simpler to measure than the free approach and the results can also be used more flexibly in case of a design change. (Fossati 2007, Larsson 2014)

In this thesis only results of simple tank tests excluding appendages and side forces are utilized. However, the CFD simulations performed in this thesis resemble the semi-captive method. The only modification to the method is the fixed pitch motion within each simulation

1.4.2 Velocity Prediction Programs (VPP)

The principles of velocity prediction of a sailing yacht have not changed for a long time. As in the area of resistance and propulsion on ships it is the force balance that is solved. The main question nowadays is how the forces are solved. In that area there are big advances made all the time.

VPP:s have long been mainly based on systematic tank test results and analytic models (Keuning et al. 1998). Within systematic tank tests the by far most extensive series is the Delft series that cover over 50 sailing yacht models (Larsson 2010). Resistance and side force prediction methods based on this series have been the most common in general VPP programs, if the project has not included own tank test or CFD computations. The methods based on the Delft series are still very widely used. The complete results of the Delft series were published in 2014 and therefore development of further methods based on the extensive tank test series is open to anyone (Keuning 2013).

On the aerodynamic side the standard method has for a long time been the Hazen aerodynamic model (Hazen 1980, Larsson 2014). It is a fairly crude model that is based on wind tunnel tests with plate sails. It gives lift and drag coefficients for five different angles for each sail individually. Extended also take into account blanketing effects, i.e. sails overlapping each other into account (Offshore Racing Congress 2012, p.42).

With the rapid development of computers, CFD analysis has become and more available to yacht designers. In America´s Cup programs and other high end racing programs it is currently a standard tool (Rosen et al. 2000). This is affecting the VPP work extensively as both hydrodynamic and aerodynamic forces can be solved to a much greater accuracy than from empirical models.

In principle it is nowadays possible to abandon the traditional VPP solver altogether and solve the whole equilibrium in a CFD software. This requires both a full hydrodynamic and aerodynamic model to be incorporated in one simulation, several degrees of freedom and at least a moving rudder to balance yaw motion. Many steps towards a fully numerical VPP have been already taken and the topic is currently researched within the sailing dynamics program in Chalmers University. A fully numerical VPP based on RANS simulations for the hydrodynamic part and a panel method for the aerodynamics was presented by at CSYS in 2005 (JACQUIN et al. 2005). Kristoph Böhm again presented a fully coupled VPP in his PhD thesis, where hydrodynamic forces are solve with a RANS code and aerodynamic forces are derived from the empirical Hazen model (Böhm 2014).

1.4.3 Computational Fluid Dynamics (CFD)

The driving factor of development within computational methods in marine hydrodynamics and aerodynamics has for a few decades now been the development of computing power. Gordon Moore of Intel predicted in 1965 that the amount of transistors on an affordable central processing unit (CPU) would double every year, meaning essentially that computer speed would double every year. He corrected his prediction in 1975, stating that the amount of transistor would double every two years. Since then his prediction has held affecting CFD development very heavily.

As the ever-developing computer power opens new possibilities for used methods and as computational results get all the time more accurate and can be solved faster, the question whether CFD will replace tank testing within marine technology has been discussed for a long time. Among others Larsson has predicted that this will happen (Larsson 1998 & Larsson et al. 2010) at some point in time. However, until present the development of CFD has also led to the development of tank test measurements, as the CFD computations are providing a competitive comparison for tank test results (Fossati 2007).

A series of workshops on the advances of CFD in ship hydrodynamics have been held since 1980. The most recent one was held in Gothenburg in 2010 with 33 groups participating from all over the world. Results on a series of test cases, that each group had computed in advance, were compared and discussed. The median of the resistance results of the test cases computed in CFD was practically zero, showing only a 0,1 % difference to the tank test results. The standard deviation of all results was 2,1 % compared to the tank test results. In the previous conference in 2005 the median was equally very close to zero, but the standard deviation was 4,7 %. Therefore a clear development in CFD accuracy could be seen over a period of five years. (Larsson et al. 2013)

Among the 33 participating CFD groups at the Gothenburg 2010 conference 22 different codes were used. Most of the simulations used Reynolds Averaged Navier-Stokes (RANS) turbulence modelling but even some Large Eddy Simulation (LES) submissions as well as one Direct Navier-Stokes (DNS) submission. The most common turbulence modelling method in the industry today is RANS, as it is more approximate in terms of turbulence modelling and requires less computational power than methods simulating turbulence in greater detail (Zou 2012). (Larsson et al. 2013)

Other main features of the Gothenburg 2010 solvers were free surface method where the Volume Of Fluid –method (VOF) almost completely had taken over, with only few submissions with a surface tracking method. Most submissions used a no-slip wall boundary conditions but also several methods with wall functions were among the submissions. Both structured and unstructured meshes were used widely. (Larson et al. 2013)

Generally the development of computer power and computational methods is giving the opportunity to explore flow phenomena faster than ever before and also it enables in depth studies in phenomena that could earlier not be investigated with empirical methods. It is now standard to solve full pressure distributions of the flow field, which might give new understanding on several phenomena. Recently, for example flows around immersed transom have been studied and new understanding on the physics affecting resistance peaks has been gained (Eslamdoost et al. 2015). On the sailing side recent research has been investigating sail and mast aerodynamics and significant differences to old empirical results have been found (Brummer 2013 & Brummer 2015).

All these studies would have been extremely difficult or impossible with empirical methods.

The future of CFD within marine applications looks very bright and the shift towards simulation based design will continue. A big shift has already happened and design processes now often include less physical testing and most off the design evaluation is done based on simulations. Physical testing is then only used at final stages of the design process for validation purposes. This again has put new demands on tank testing procedures and their accuracy. Simulation is now used in all areas of hydrodynamic design. These include among others resistance and propulsion, seakeeping, manoeuvring and stability and capsize. With the development of computational power and CFD tools computational hydrodynamics is bound to expand and become broadly available. The tools will enable engineers to design safer, innovative and cost saving solutions to meet the challenges of the 21st century. (Stern et al. 2012)

1.5 Objective of the Thesis

The aim of this thesis is to computationally define optimal sailor position in flat water conditions taking the full sailing equilibrium, i.e. both hydrodynamic and aerodynamic as well as gravitational forces, into account. Also, the VPP results of this thesis will serve as a reference for future research within sailing dynamics. No optimization algorithms will be used, but the optimal sailing conditions will be sought through a manual process of evaluating several sailing conditions and identifying the optimal ones. The study will be performed based on tank test results, VPP calculations and CFD simulations.

As the Laser dinghy is one of the most sailed boats in the world, it is not expected that this thesis would produce any revolutionary news of sailor positioning in a completely new manner. However, it will increase our understanding on the physics behind chosen sailing techniques and might give some ideas to test out on the water. Also it will advance the science of sailing, as common methods within yacht design are evaluated based on CFD simulations and tank tests.

1.6 The Laser

The test case in this study is the Laser Standard dinghy which is the men´s one person Olympic sailing class at present. The Laser was first designed and built in 1970 and officially unveiled at the New York Boat Show in 1971. The Laser has held the Olympic status since 1996.

The Laser is a simple construction with a glass fibre hull, glass fibre appendages, an aluminium mast and a Dacron sail. It can easily be sailed even by a beginner. As the dinghy has no keel weight adding stability, the righting moment of the boat is mostly produced by the sailor hiking from the hiking straps.

The hull weights approximately 59kg and with all gear the boat weights approximately 82kg. Competitive sailors weigh normally 80-84kg. The length of the boat is 4,21m and the beam is 1,37m. The sail area is 7,06m^{2}.

The Laser in action can be seen in Picture 1. The mast bends relatively heavily backwards when the boat is sailed. The force to bend the mast is produced with the sheet that is attached to the boom. When the sail is sheeted in and the mast therefore as well bent, the sail adopts it´s correct shape. A 3D-model of the Laser is shown in Figure 1. The hull and appendages are the same as used for the simulations.

Picture 1 Laser upwind sailing

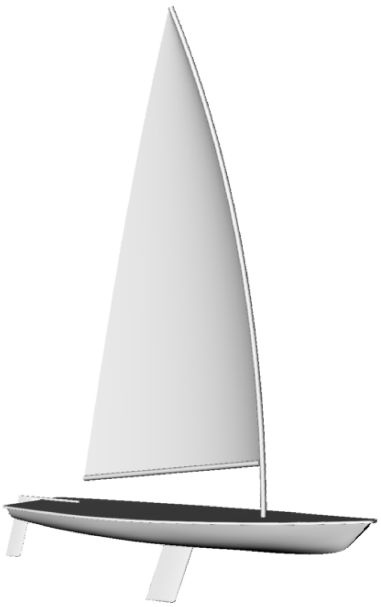

Figure 1 A 3D-model of the Laser

1.7 Limitations

In this thesis flat water is assumed and only upwind cases are addressed. The assumption of flat water is realistic in light winds and the study concentrates on the light wind range up to approximately eleven knots of true wind speed. This wind strength correlates to the maximum boats speed. Above this wind speed the boat speed does not increase at all or very little. However the rig aerodynamics would change significantly and waves would change the hull hydrodynamics.

Downwind could be addressed to some extent based on the tank test results used in this thesis. The simulations of this thesis are however not applicable to downwind cases as the leeway that is needed for upwind cases not only changes the appendage hydrodynamics but also the hull hydrodynamics.

2 Inverse Velocity Prediction Program (IVVP)

2.1 Procedure

In this chapter the procedure of the thesis and tools used will be explained. First an overall picture of the whole process will be given and then the steps will be clarified in greater detail. A flow chart of the process of this study is shown in Figure 2.

As a starting point for the study full scale tank test results earlier performed on the Laser at SSPA were used. Based on the results of the tank tests a preliminary overall picture on the resistance behaviour of the Laser was formed. Important factors were how the resistance would change as a function of trim and heel. Further, the tank test results were used as a starting point for the first Inverse velocity prediction program calculations (IVPP).

Next a first round of IVPP calculations was performed to obtain as accurate as possible estimates for sailing conditions. These estimates were used to define the matrix of CFD simulations. A matrix of CFD simulations was then performed to obtain accurate hydrodynamic data for final IVPP calculations.

Finally a second round of IVPP calculations was performed. From the IVPP results as well as CFD simulations optimal heel and trim angles as well as sailor positions were solved.

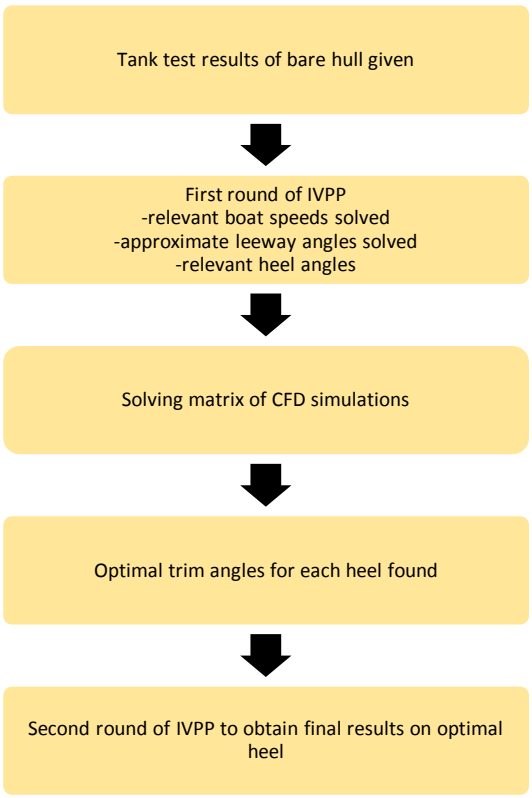

Figure 2 Process of the study

2.2 Use of Tank Test Results

The tank tests served as an initial guess on optimal trims and heel angles as well as validation cases for the CFD simulations.

There was no exact knowledge on whether or not the flow field or resistance characteristics underneath the hull would change dramatically enough to change either optimum trim or the heel characteristics. These together with the sail forces would define optimal heel conditions for different boat speeds and winds.

From the tank tests it was possible to plot the change of resistance as a function of heel and compare this to sail forces also plotted against heel. By this comparison initial guesses of relevant areas of possible optimum trim could be found. An example of this principle is shown in Figure 3. The optimum heel in the example would be found around ten degrees of heel, where the difference between drive and resistance is largest. In practice this would mean that as certain speed of the example would be achieved by the smallest possible wind strength at the heel of ten degrees.

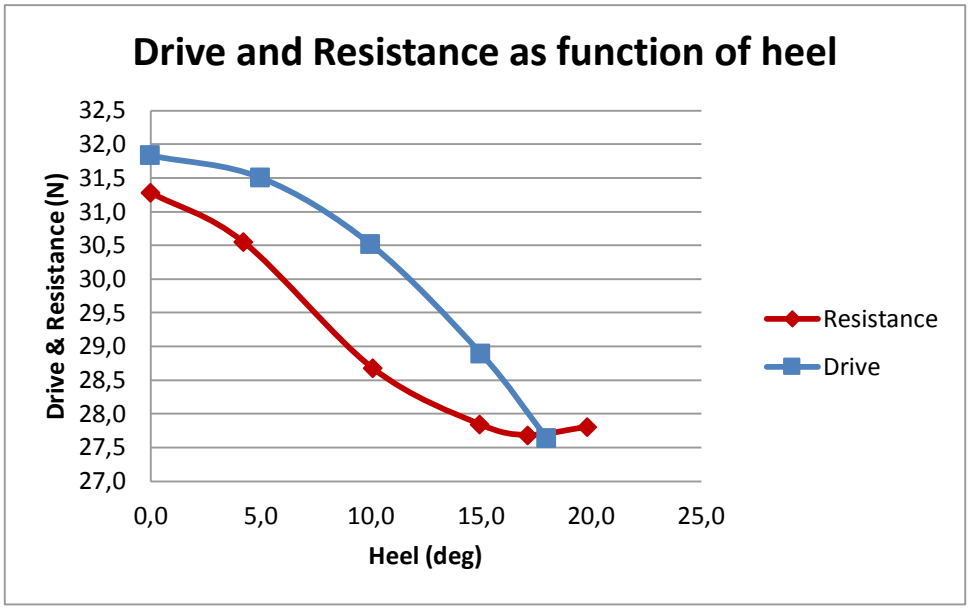

Figure 3 Principle of finding optimal heel where the difference of drive and resistance is largest

2.3 Principles of the Inverse Velocity Prediction Program

A special purpose VPP program was made within this study by the author. The main characteristic of the program is that it solves the sailing equilibrium inversely to a typical VPP program. Therefore it is called Inverse Velocity Prediction Program (IVPP). Typically in VPPs the input is the wind and the resulting boat speed is solved. In the IVPP the input is the boat speed and the required wind is solved. As by-products the leeway angle and sailor position are solved for each combination of speed and heel angle. The computation of ideal trim is not included in the IVPP, but is computed outside it within the matrix of CFD simulations.

The advantage of the IVPP compared to a typical VPP in this study is the lack of interpolation between speeds. This increases the accuracy of the study as interpolation within the highly non-linear resistance curve would be unnecessarily approximate. Adding simulated speeds again was not an option, as the amount of simulations for each speed needed in this study is large.

The IVPP consists of two modules, the aerodynamic module and the hydrodynamic module. In the first round of IVPP calculations leeway angles and ideal heel angles were solved based on the hydrodynamic data from the tank tests and addition of forces on appendages based on analytic methods. The results of the first round of IVPP calculations were used do define the matrix of CFD calculations. The principle of the first round of IVPP calculations is shown in the flowchart in Figure 4.

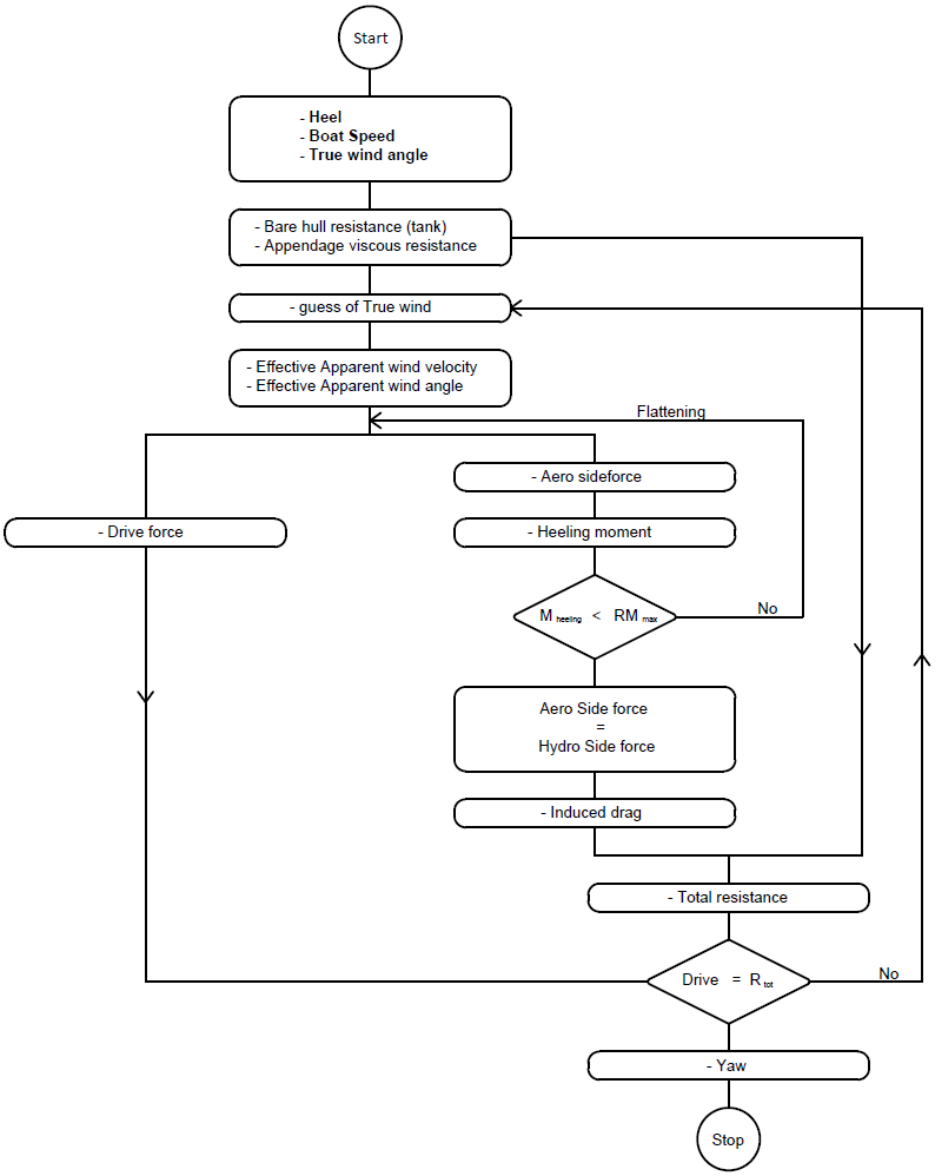

Figure 4 IVPP, first round based on tank tests and analytic calculations

In the second round of IVPP calculations the matrix of CFD computations was already solved and the obtained data could be used as the hydrodynamic input for the IVPP. Still the same analytic methods for appendages as in the first round of IVPP calculations were used, but this time only for small corrections to obtained hydrodynamic data from CFD simulations. The principle of the second round of IVPP calculations is shown in the flowchart in Figure 5.

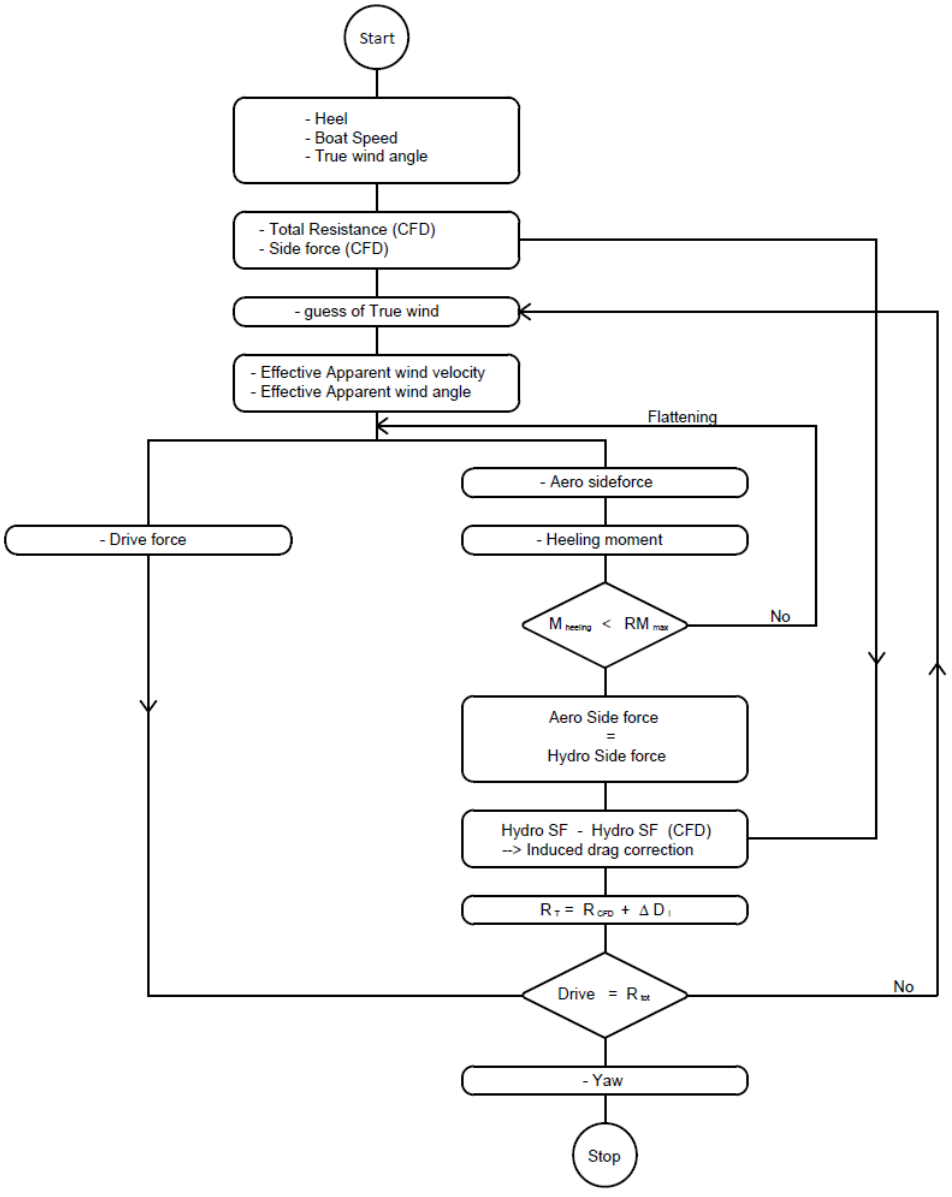

Figure 5 IVPP, second round based on CFD computations and analytic corrections

In the following chapters the principles of the IVPP are explained in more detail. First the forces and moments acting on a sailing boat are presented and the calculation of the forces is introduced.

2.4 Balance of Forces and Moments

The foundation of sailing yacht physics is the force balance between aerodynamic and hydrodynamic forces. This balance is often also referred to as the sailing equilibrium, or the symmetry of sailing.

When all forces and moments on a yacht find their equilibrium, the yacht will move through the water with a constant speed, heel angle and yaw angle. The water surface can be thought as a kind of symmetry plane, as the aerodynamic forces act forward and leeward whereas the hydrodynamic forces counterbalance the aerodynamic forces by acting backwards and windward.

Going upwind the sails have a small angle of attack and work like lifting wings. In downwind conditions the sails are close to perpendicular to the wind and work as drag plates.

The real forces from the sails, appendages and hull are more often than not at complex angles in space. However, these forces are handled in two different coordinate systems that can relatively easily be related to each other. The first one is a Cartesian coordinate system tied to the boat and heeling and pitching with it. The second one is the global Cartesian coordinate system with the x-axis pointing in the direction of the yachts forward motion.

The force pairs to balance are (Larsson et al. 2014, p.69-70):

Aerodynamic Drive - Hydrodynamic Resistance
Aerodynamic Side Force - Hydrodynamic Side Force
Weight of the boat - Buoyancy Force

And the Moments to balance are (Larsson et al. 2014, p.69-70):

Heeling moment - Righting moment
Aerodynamic trimming moment - Hydrodynamic trimming moment

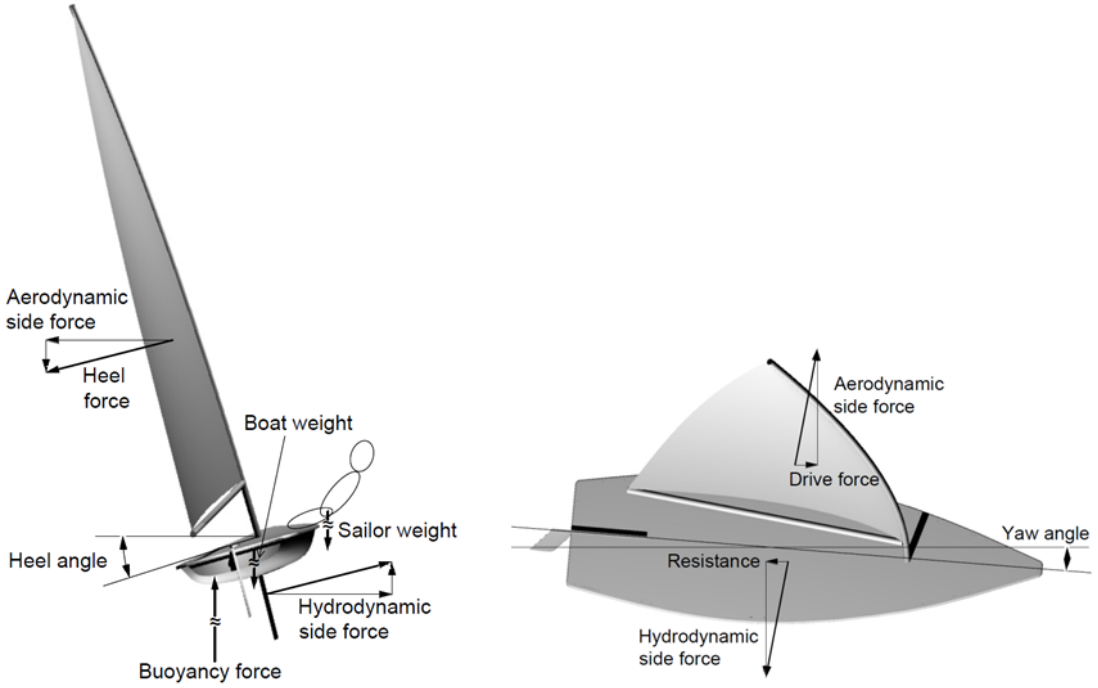

Figure 6 Force balance on a sailing boat

To determine a sailing yachts speed, one has to know at what speed the specific forces occur. When the resistance curve of the yacht is known the corresponding speed to a specific case of equilibrium with a specific side force can be determined.

2.5 Aerodynamic Forces – Hazen´s Method

In this study Hazen´s aerodynamic model (Hazen 1980) is used to estimate the sail forces within the IVPP. Hazen´s aerodynamic model is based on empirical measurements, where sail forces were measured on a sailing yacht in real sailing conditions. The hull used was a thoroughly tank tested model, and therefore this hull could be used as a dynamometer as it´s behaviour was known. Lift and drag coefficients are given for the main sail, jib, spinnaker, mizzen and a mizzen stay sail. The model is made to cover diverse rig types, but it only gives one set of lift and drag coefficients for each sail. Therefore as the sails interfere with each other in different rigs in different ways, there will be a relatively large margin of error in the sail power estimates. Still the model also includes formulae to take blanketing effect into account. In the case of the Laser Olympic sailing dinghy (Laser) these effects are not relevant as the Laser only has one sail.

Hazen´s aerodynamic model has long been a standard to derive sail forces and has widely been used in VPP-programs. However, as CFD simulations have given much added information during recent years it is nowadays known that the model is relatively crude. Despite of this, it is still the most significant and used aerodynamic model within VPP programs.

In the case of this study the most critical effects in terms of correct results are not related to the absolute values of sail forces, but rather the change of sail forces when the boat is heeled. This is largely a geometrical correlation (Larsson 2014) and can be solved with basic trigonometry.

2.5.1 Geometry

The Hazen model treats sails as triangles from corner to corner and therefore neglects roach both in the front and in the back of the sail. The sail area A_{Sail} is defined below, where *P* is the luff length and *E* the foot length of the sail.

$$A_{Sail} = 0{,}5 \times P \times E$$

The Centre of effort is taken as 39 % of the luff length. As the laser sail is heavily raked backwards the centre of effort in this study is taken as 39 % of the length of the line that runs from the middle of the boom to the top of the sail. The centre of effort *CE* is defined below, where P is the luff length and *BAD* is the distance from the deck to the sail foot (boom above deck).

$$CE = 0{,}39 \times P + BAD$$

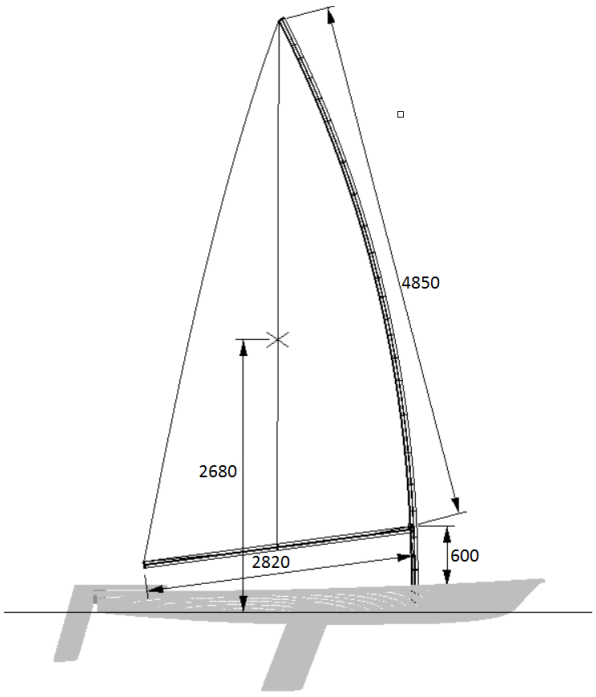

Figure 7 Laser rig dimensions

2.5.2 Lift Coefficient

The Hazen method gives coefficients for lift and drag that are derived from wind tunnel tests. The coefficients have been derived for relatively few angles but interpolation through the whole range of angles has been general practice within yacht design. In this study very little interpolation is needed as only one upwind angle is investigated. The true wind angle throughout this study is 45 degrees, and the apparent wind angle varies from approximately 27 to 30 degrees.

Hazen Sail Coefficients for main sail

Apparent wind angle	Lift	Viscous Drag
27	1,5	0,02
50	1,5	0,15
80	0,95	0,8
100	0,85	1
180	0	0,9

Table 1 Hazen Sail coefficients

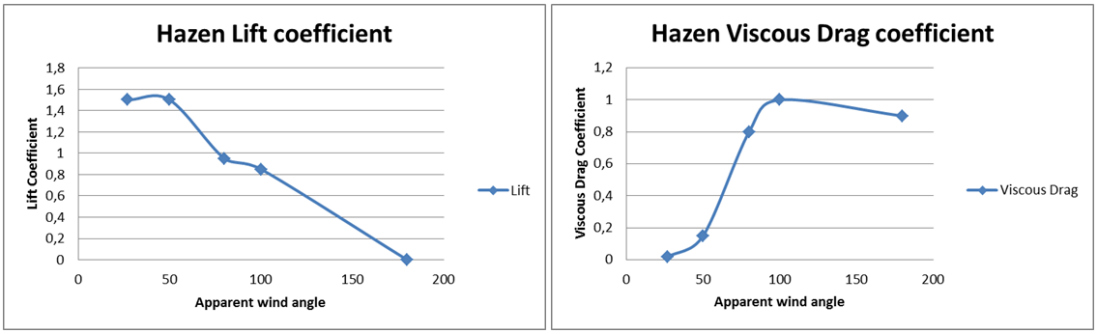

Figure 8 Hazen sail coefficients graphically

2.5.3 Induced Drag

As is common in other methods too, in the Hazen´s method the induced drag is regarded proportional to the lift squared and inversely proportional to the aspect ratio of the sail. However in Hazen´s method a constant factor of 0,005 has been added to the formula. The factor stands for a viscous part of the total drag that Hazen claims to be proportional to Cl^2 in the same manner as the induced drag. The induced drag coefficient Cd_i is defined below, where Cl is the lift coefficient and AR the aspect ratio of the sail.

$$Cd_i = Cl^2\left(\frac{1}{\pi \times AR} + 0{,}005\right)$$

2.5.4 Aspect Ratio

The aspect ratio for close hauled sailing conditions in Hazen´s model is defined as a stretched version from the geometrical aspect ratio and a luff length measured from the waterline to the mast top is used. Also this length is then multiplied by a factor of 1,1. As the aerodynamic planform of the sails is stretched all the way to the waterline, it seems that the method assumes the sails to be attached to the deck. Also the factor of 1,1 indicates an end plate effect of the water surface. The aspect ratio AR is defined below, where EHM is the mast height above the sheer line, FA is the average freeboard height and A_{Sail} is the sail area.

$$AR = \frac{(1{,}1 \times (EHM + FA))^2}{A_{Sail}}$$

Hazen´s model however is made for sail combinations with jibs all the way to the deck. The Laser has a boom that is very clearly detached from the hull and has no foresail. Therefore a slightly different approach was taken to the calculation of aspect ratio. The aspect ratio for the Laser in this study is taken as the geometrical aspect ratio, i.e. the ratio of the luff length to the mean chord of the sail. Therefore the extension to the waterline and the end plate effect are not accounted for. This should be a more realistic method in the case of the laser essentially it makes the sail less effective creating more side force compared to drive force than a higher aspect ratio. The aspect ratio of the Laser is defined below as AR_{Laser}, where P is the luff length and E the foot length of the sail.

$$AR_{Laser} = \frac{P}{E} \times 2$$

2.5.5 Drag of Mast and Topsides

The drag coefficients of the mast and topsides are defined as 1,13. It is known, that the wind close to the sea level is lighter than the wind higher up (Tennekes 1972), and therefore using the apparent wind velocity and same drag coefficients could be questioned. Also, it has become evident during the CFD era, that the mast provides a significant amount of drive force (Brummer 2015), which is not accounted for in the Hazen model. However there are many simplifications in Hazen´s model and used as an entity, it has proven to give reasonable accuracy. Therefore no modifications are made regarding the drag of mast and topsides.

The drag of the topsides and the mast is calculated according to the frontal area of the boat and mast.

2.5.6 Flattening

Flattening is a depowering factor of the sail used in Hazen´s model. If no flattening is used the factor is 1. The smaller the factor gets the bigger the flattening effect is. To use

flattening Cl is multiplied with a factor F. The smallest possible flattening factor was regarded as 0,6 in this study.

As the induced drag coefficient Cd_i is related to the square of the lift coefficient Cl^2, the flattening factor will reduce induced drag significantly. Therefore by flattening the sail the proportion between lift and drag or effectively drive force and heel force will become more favourable. When the heeling moment reaches the maximum righting moment and a sail must be flattened to keep the balance. As the proportion of drive force and heel force becomes more favourable, speed is not necessarily reduced due to the reduced forces. The correlation of induced drag and lift is later discussed presented in this chapter.

2.5.7 Calculation of Total Lift and Drag

The lift of the sail which is directed at right angles to the apparent wind is defined below as L_{Sail}, where ρ is the density of air, V_{AW} is the apparent wind speed, A_{Sail} is the sail area and Cl is the lift coefficient.

$$L_{Sail} = \frac{1}{2}\rho {V_{AW}}^2 A_{Sail} Cl$$

In a similar manner the drag components can be calculated using the respective area and drag coefficient for each drag component. All drag components are directed in line with the apparent wind. The Drag components are calculated as follows, where D is drag, ρ is the density of air, V_{AW} is the apparent wind velocity, A is the respective area for each drag component and C_d is the respective drag coefficient for each drag component.

$$D = \frac{1}{2}\rho {V_{AW}}^2 A\, C_d$$

This concludes the Hazen´s aerodynamic model in the case of the Laser. The model has far more coefficients for other sails and methods to take blanketing that are not presented here, however these are not relevant for the simple case of the Laser.

2.6 Hydrodynamic Forces on Appendages

To solve the sailing equilibrium the IVPP needs be able to solve the hydrodynamic forces acting on the boat hull and appendages. In this study two different methodologies are used for this. In the first round of IVPP calculations the forces are calculated combining the tank test data and forces on appendages estimated by analytic formulae. In the second round of IVPP calculations the hydrodynamic forces are solved with the CFD code Star CCM+ and corrected with analytic formulae in case of the hydrodynamic side force not matching the aerodynamic side force. The analytic formulae used are the same in both steps and is presented in the following paragraphs.

2.6.1 Frictional Resistance

The Reynolds number is a dimensionless quantity that is defined as the ratio between momentum forces and viscous forces. The Reynolds number is defined below where $V = \text{velocity}, L = c\text{haracteristic length}, \rho = \text{density}, \nu = \text{kinematic viscosity}, \quad \mu = \text{dynamic viscosity}$

$$R_n = \frac{VL}{\nu} = \frac{\rho VL}{\mu}$$

The ITTC-57 friction line is an empirical formula developed by the International Towing Tank committee (ITTC 2000). The result is the non-dimensional friction coefficient C_f. The formula is developed for ship hulls but is widely also used for appendages. The ITTC-57 friction line is defined below, where $R_n = \text{Reynolds number}$

$$C_f = \frac{0{,}075}{(Log\ R_n - 2)^2}$$

The frictional resistance is therefore given as below, where $\rho = \text{density}, V = \text{velocity}, S_W = wetted\ surface, C_f = \text{friction coefficient}$

$$R_f = \frac{1}{2}\ \rho\ V^2\ S_W\ C_f$$

2.6.2 Viscous Pressure Drag

The viscous pressure drag around a moving boat or ship is often defined with a form factor. The form factor is normally given as a 1+k value, where k defines the portion defines a pressure drag that is proportional to the frictional drag. To estimate the pressure drag on the foils in this study the Hoerner form factor (Hoerner 1992) was used. The Hoerner form factor is defined below, where $t = \text{thickness}, c = \text{chord}$

$$(1 + k) = 1 + 2\frac{t}{c} + 60\left(\frac{t}{c}\right)^4$$

2.6.3 Induced Drag

The induced drag, also called drag due to lift is the additional drag caused when a wing creates lift. When a wing creates lift it turns the airflow. The lift will be perpendicular to the turned flow direction and therefore include a component pointing backwards, the induced drag.

The induced drag coefficient is defined below as presented by John D. Anderson (Anderson 2010), where $Cl = \text{lift coefficient},\ A_e = \text{effective aspect ratio}$

$$Cd_i = \frac{Cl^2}{\pi A_e}$$

According to lifting line theory (Katz et al. 2001) the lift curve slope of 2D and 3D wings are given as below, where $Cl = \text{lift coefficient},\ A_e = \text{effective aspect ratio}$

$$\frac{dCl}{d\alpha_{2D}} = 2\pi$$

$$\frac{dCl}{d\alpha_{3D}} = \frac{2\pi}{1 + \frac{2}{A_e}}$$

Therefore lift and induced drag are defined as below, where $\rho = \text{density},\ V = velocity,\ S = \text{planform area}, Cl = \text{lift coefficient}, Cd_i = \text{induced drag coefficient}$

$$Lift = \frac{1}{2}\rho V^2 S Cl$$

$$D_i = \frac{1}{2}\rho V^2 S Cd_i$$

The aspect ratio of a wing is defined as below, where $b = \text{span},\ C_m = \text{mean chord},\ S = \text{planform area}$

$$AR = \frac{b}{C_m} = \frac{b^2}{S}$$

The center of lateral resistance (CLR) taken as 45 % of the depth (Gerritsma 1985).

2.7 Induced Drag Factor

The induced drag factor is a measure used to measure the ability of a yacht to produce side force. The more effective the yacht is the less induced drag the yacht produces for a give side force. The concept is explained more in detail in the following paragraphs.

When a wing has zero angle of attack it will only experience frictional and viscous pressure drag. Once the wing is set at an angle of attack to the incoming flow a pressure difference between the sides of the wing will be created. This pressure difference causes both lift and an additional drag component – induced drag. Due to its close relation to lift this drag component is often also called *drag due to lift*. (Anderson, 2001)

As can be shown from potential flow theory, the induced drag is directly related to the square of lift.

$$Cd_i = \frac{Cl^2}{\pi A_e}$$

The keel of a yacht or the centreboard of a dinghy can be seen as finite wings with a mirror boundary at the top end. Therefore the same principles apply for keels and centreboards as for any other wings. Interestingly, also the hull of a yacht or dinghy that partly contributes to the side force produced follows the same principles. Therefore the side force produced by a sailing boat can be plotted against the drag as shown in Figure 9.

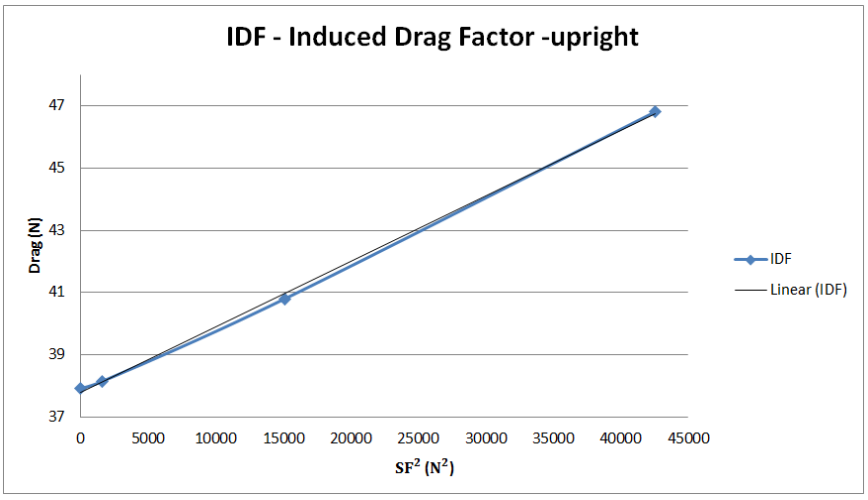

Figure 9 Linear correlation of Resistance to side force squared

The steepness of the plot tells how effectively a yacht produces the side force needed. The flatter the graph is, the more effective the production of side force. The slope of the plot is called the Induce Drag Factor or just IDF.

The IDF graph in Figure 9 is based on CFD simulations during verification simulations. The graph shows a very close fit to the theoretical linear correlation between the square of the side force and drag.

2.8 Geometric Correlations

When forces on a sailing yacht are evaluated or a VPP is built, there are two Cartesian coordinate systems that have to be dealt with. Both coordinate systems have their x-axes in the direction of motion of the yacht, but one is always upright while the other one heels with the boat having its xy-plane always perpendicular to the mast if the mast is positioned straight on the boat with no forward or aft rake.

All forces produced by the sails and the keel are easiest solved in the heeled coordinate system whereas the final force balance to determine the boat´s speed is easiest solved in the upright coordinate system.

As the boat in reality is heeled, it is important to solve the aerodynamics and hydrodynamics in the heeled plane as the forces acting on the sails are determined by the flow components in this plane (Kervin 1978). To start with, the inflow has to be understood. As the boat is heeled the apparent wind has to be solved in the heeled plane. This wind component is called the effective apparent wind. The effective apparent wind consists of the longitudinal component of the apparent wind and the transversal component of the apparent wind being perpendicular to the mast and sails (Campbell et al. 1994, Jackson 1996). This is illustrated in Figure 10.

V_1 is the longitudinal component of the apparent wind. $V_\square$ is the transversal component of apparent wind in the upright coordinate system. V_2 is the transversal component of the apparent wind being perpendicular to the mast and sails. V_{AW} is the apparent wind in upright coordinates and V_{EAW} is the effective apparent wind in heeled coordinates.

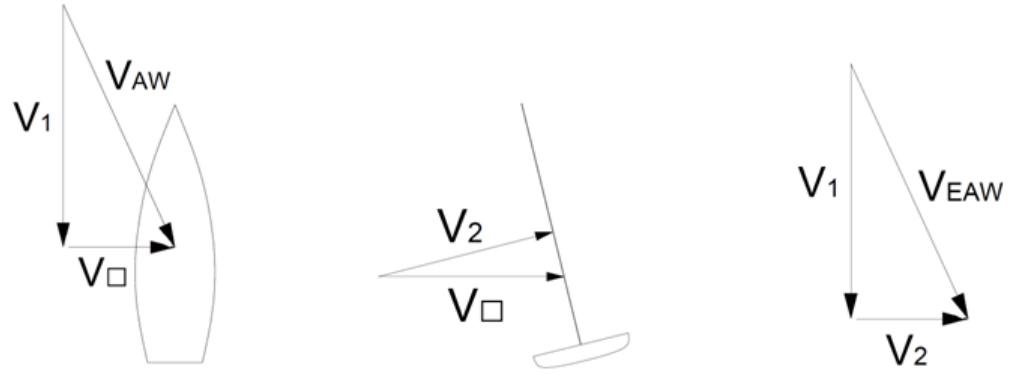

Figure 10 Wind components to solve effective apparent wind

The effective apparent wind is the wind used for all aerodynamic calculations. The same procedure is also applied for the appendages that are similarly experiencing a change of effective water inflow as a function of heel. Finally, when aerodynamic and

hydrodynamic forces have been solved in the heeled coordinates their upright components can be solved and the full force and moment balances established. As a result the required wind speed for a certain seed can be solved or vice versa, the speed of the yacht achieved with a certain wind strength and angle.

3 Computational Fluid Dynamics (CFD) Simulations

3.1 Matrix of Flow Simulations

Returning to the main process of the thesis this chapter will introduce the matrix of flow simulations performed and explain how the simulations were chosen

The purpose of the flow simulations in this study was to find the optimal trim angle for each heel angle as well as solving the relation of resistance and side force for each case correctly. The first round of IVPP calculations indicated approximately the relevant heel angles and gave a first estimate on the leeway angles to achieve the side forces needed for each case. The relevant trim angles were estimated from the preliminary tank tests and aimed to cover trims both below and above the optimum trim.

The matrix of simulations was then created over the whole upwind speed range from two to five knots boat speed. Within each speed, heel and trim were systematically varied. The yaw angle was kept constant within each speed, always using an estimate on the yaw angle indicated by the first round of IVPP calculations. As an exception only one trim was investigated in the speed of two knots as the trim in low speed is restricted by the class rules forbidding any body parts to be in front of the mast. The full matrix of CFD simulations is shown in Figure 11.

Only one trim angle and five heel angles in 2kn boat speed

Three heel angles for speeds 3, 4 and 5kn

A minimum of four trim angles for each heel

YAW 3,7			2kn Drags				2kn SF			
Heel	Trim	Yaw	Hull	CB	Rudder	Total	Hull	CB	Rudder	Total
0	2	3,7	6,6	1,83	1,11	9,5	4,79	25,83	3,18	33,81
5	2	3,7	6,6	1,70	1,11	9,4	3,92	24,19	3,64	31,75
10	2	3,7	6,3	1,61	1,02	8,9	4,14	21,55	3,19	28,87
15	2	3,7	5,95	1,59	0,95	8,5	3,83	18,09	2,35	24,26
18	2	3,7	5,72	1,62	0,91	8,3	3,39	16,44	1,69	21,52

YAW 3,7			3kn Drags				3kn SF			
Heel	Trim	Yaw	Hull	CB	Rudder	Total	Hull	CB	Rudder	Total
0	-1	3,7	15,57	4,93	1,91	22,4	7,5	60,6	12,6	80,7
0	-0,5	3,7	14,8	4,83	2,18	21,8	7,6	60	12,5	80,1
0	-0,25	3,7	14,6	4,77	2,34	21,7	7,7	59,7	12,1	79,5
0	0	3,7	14,6	4,71	2,49	21,8	7,9	59,8	11,4	79,1
0	0,5	3,7	14,95	4,62	2,80	22,4	8,1	59,3	10,2	77,6
8	-0,5	3,7	14,8	4,64	1,97	21,4	8,6	61,2	4,5	74,2
8	0	3,7	14,5	4,52	2,26	21,3	8,9	59,7	6,3	74,9
8	0,5	3,7	14,7	4,38	2,45	21,5	9	58,0	8,1	75,1
8	1	3,7	15,1	4,25	2,45	21,8	9,2	56,4	8,5	74,1
8	1,5	3,7	15,5	4,10	2,32	21,9	9	55,0	7,5	71,4
16	0	3,7	13,5	4,69	1,91	20,1	7,1	53,7	3,4	64,2
16	0,5	3,7	13,4	4,52	1,91	19,8	7,4	50,4	4,1	61,9
16	1	3,7	13,6	4,35	1,89	19,9	7,8	46,9	5,6	59,2
16	1,5	3,7	13,9	4,16	1,83	19,9	7,2	43,4	4,9	55,4
16	2	3,7	14,3	3,99	1,74	20	7,0	40,4	4,4	51,8

Yaw 4,0			4kn Drags				4kn SF			
Heel	Trim		Hull	CB	Rudder	Total	Hull	CB	Rudder	Total
0	-0,5	4	30,95	8,67	3,17	42,8	18,4	117,16	20,33	155,9
0	-0,25	4	30,9	8,59	3,25	42,7	18,76	116,79	20,24	155,8
0	0	4	30,95	8,54	3,3	42,8	19,17	117,31	19,72	156,18
0	0,5	4	31,75	8,34	3,47	43,55	19,46	116,28	18,9	154,65
7	-0,5	4	32,1	8,42	2,68	43,2	21,2	122,2	6,4	149,7
7	0	4	31,6	8,20	2,82	42,6	21,8	120,1	5,3	147,2
7	0,5	4	31,8	7,93	3,10	42,8	21,7	117,8	5,9	145,5
7	1	4	32,9	7,64	3,47	44,0	22,0	115,4	10,1	147,4
7	1,5	4	34,3	7,39	3,65	45,4	22,4	112,8	13,2	148,3
14	0	4	30,3	8,12	2,96	41,3	19,0	105,6	4,3	129
14	0,5	4	30,3	7,86	3,06	41,3	19,8	105,4	6,2	131,5
14	1	4	30,8	7,52	3,06	41,4	20,2	102,9	7,0	130,2
14	1,5	4	31,7	7,14	3,04	41,8	20,3	98,6	8,0	126,9
14	2	4	33,0	6,74	2,97	42,7	20,3	93,6	8,2	122,1

Yaw 4,65			5kn Drags				5kn SF			
Heel	Trim	Yaw	Hull	CB	Rudder	Total	Hull	CB	Rudder	Total
0	0	4,65	70,3	14,98	5,61	90,9	41,7	215,2	36,0	292,8
0	-0,5	4,65	68,6	15,09	5,84	89,5	40,1	214,5	38,5	294,0
0	-1	4,65	68,3	15,25	5,97	89,5	40,2	214,3	40,4	295,0
0	-1,5	4,65	69,2	15,39	6,08	90,6	38,8	213,4	41,6	293,8
0	-2	4,65	71,7	15,53	6,14	93,3	37,7	212,4	42,4	292,5
0	-2,5	4,65	75,4	15,68	6,16	97,2	42,1	212,3	36,5	291
5	0	4,65	72,4	14,76	4,96	92,1	46,5	216,4	22,0	285,0
5	-0,5	4,65	71,1	15,08	5,17	91,4	45,5	218,7	24,6	288,8
5	-1	4,65	70,9	15,3	5,34	91,6	44,3	219,7	26,2	290,2
5	-1,5	4,65	72,1	15,57	5,52	93,2	42,8	220,7	28,49	292,0
5										
10	0	4,65	73,7	14,66	4,51	92,8	48,2	207,5	12,7	268,3
10	-0,5	4,65	73,1	15,14	4,62	92,9	46,9	210,9	14,2	272,0
10	-1	4,65	73,8	15,55	4,83	94,2	44,9	213,6	17,1	275,5
10	-1,5	4,65	75,5	15,99	4,96	96,4	43,1	217,0	18,2	278,3

Figure 11 Matrix of CFD simulations

InFigure 11 Matrix of CFD simulations Figure 11 it can be seen that the matrix consist of four main parts in vertical direction. These parts represent the four boat speeds from two to five knots. The first part is smaller than the others, as it does not contain any variation of trim. For each speed there are eleven columns. The three first columns indicate the heel, trim and yaw angles, i.e. define the geometrical constraints. The next four columns show the resistances of the hull, centreboard and rudder separately and finally the sum of these. Similarly the data for side forces is shown in the last four columns.

For each speed, except for 2kn, there are always three groups of rows. The groups always have constant Heel angles, but the trim is systematically varied within them. The groups have different heel angles compared with each other. In this way a matrix with systematically varying speed, heel and trim was created.

3.2 Simulation Setup

When a flow problem is solved, the control volume, also called the domain, has to be defined. At the edges of it boundary conditions have to be defined and normally the area of interest will be somewhere in the middle of the domain. There are many different methods within Computational fluid dynamics but most methods are of Eulerian type where the inflow and outflow of a control volume is studied. Also the Reynolds-Averaged Navier-Stokes method used in this study is of this type. The computational domain is further divided into small cells, each being a control volume. This system of cells is called a grid or a mesh. Within the mesh, the flow within each cell will be solved and the flow problem becomes a system of equations where each cell is affected by its neighbouring cells. The more cells the computational mesh has, the longer the simulation will take. Therefore it is essential to use an as coarse mesh as possible without losing accuracy.

The simulations in this study were done using the RANS based computational fluid dynamics (CFD) solver Star CCM+. Star CCM+ is a general purpose CFD code and is made to be very flexibly utilised within different flow phenomena. In the case of this study an external two phase flow including the free surface simulation was solved. The free surface was treated with the Volume of Fluid –method where each cell is given a volume fraction that describes the amount of water and air within that specific cell. The turbulence model used was the SST K-Omega model.

The control volume in this external flow case around the Laser was box shaped extending approximately one boat length in front of the boat, four boat lengths behind the boat, one boat length below the boat and 1,5 boat lengths on each side of the boat. The grid is very dense around the hull and appendages as well as between the appendages. The grid then coarsens highly towards the edges of the computational volume both reducing the total cell amount and deflection of pressures from the edges. To allow for the movement of the boat during the simulation an overset mesh was used. This is further explained later in Figure 14. The grids used contained approximately seven million cells. The computational mesh and the effect of its density on the wave pattern are further explained in Figure 12 to Figure 15.

The grids used for the CFD calculations were created using Star CCM+´s trimmer meshing tool that creates unstructured hexagonal meshes. Grids built with the trimmer meshing tool have sides of the hexagonal cells that are aligned with the coordinate system, which is advantageous as the flow also is highly aligned with one of the axes, the one longitudinally with the boat.

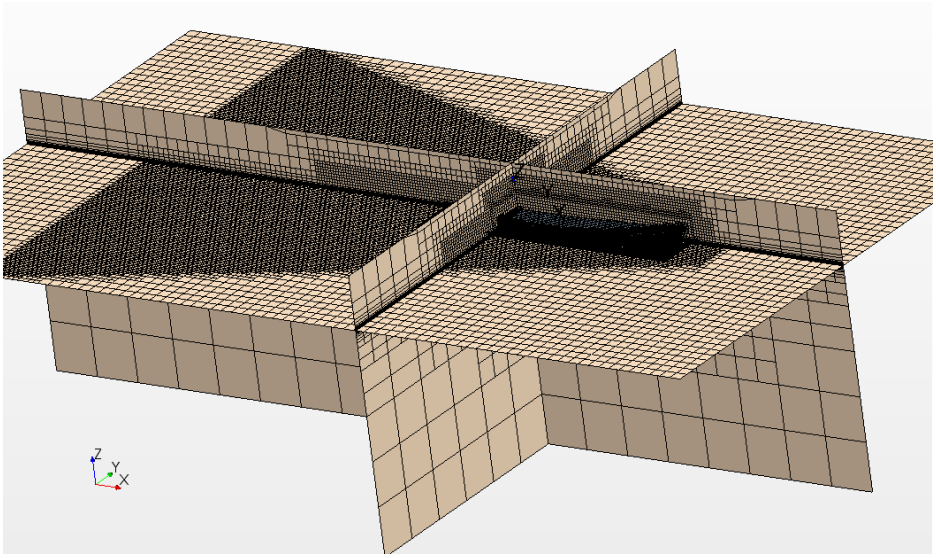

Figure 12 Cross sections of the whole computational domain

Figure 12 shows cross sections of the whole computational domain. It can be seen that the mesh is very dense close to the boat and coarsens to the edges of the domain. The relevant areas of the flow field also further away from the boat have a relatively dense mesh. The characteristic triangle seen in Figure 12 is the dense area of the mesh around the wave pattern created by the boat at the free water surface. It is important that the mesh is dense enough to capture the wave pattern with reasonable accuracy. The thickness of the denser part to capture the wave pattern is adjusted for each speed depending on the wave height.

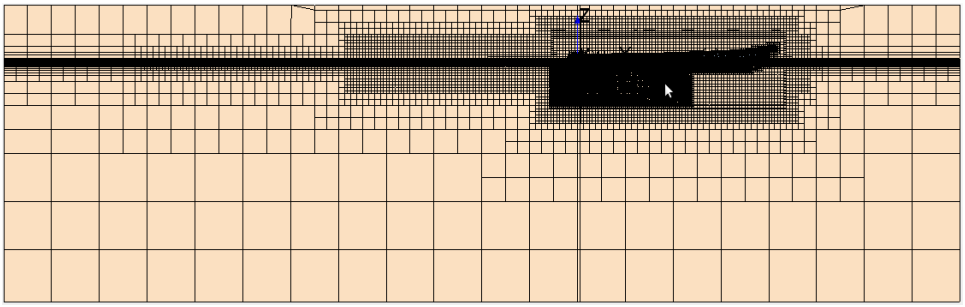

Figure 13 Side view of the whole computational mesh

In Figure 13 the whole computational mesh can be seen in a side view. The coarsening of the mesh towards the sides of the domain is very apparent. Also the denser grid close to the free water surface can clearly be recognized. The appendages cannot be seen in the figure, but the dense grid around them and between them can clearly be seen.

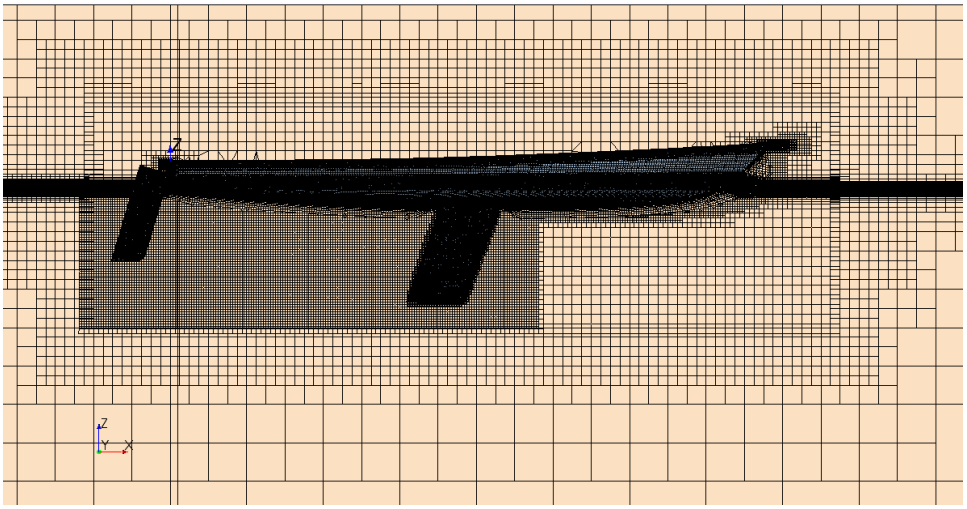

Figure 14 Side view of the computational mesh close to the boat

Figure 14 shows a close up of the same computational mesh than in Figure 12 and Figure 13. Here the edges of the overset mesh on each side of the boat can be seen as a rectangular frame that is denser than the grid inside or outside the frame. This is the overlapping area of the overset mesh and the domain mesh. The overset mesh can move relative to the domain mesh during the simulation. In the simulations performed the boat was free to heave and therefore features of the mesh that were specifically adjusted to the boat hull would move with the overset mesh that is fixed to the hull.

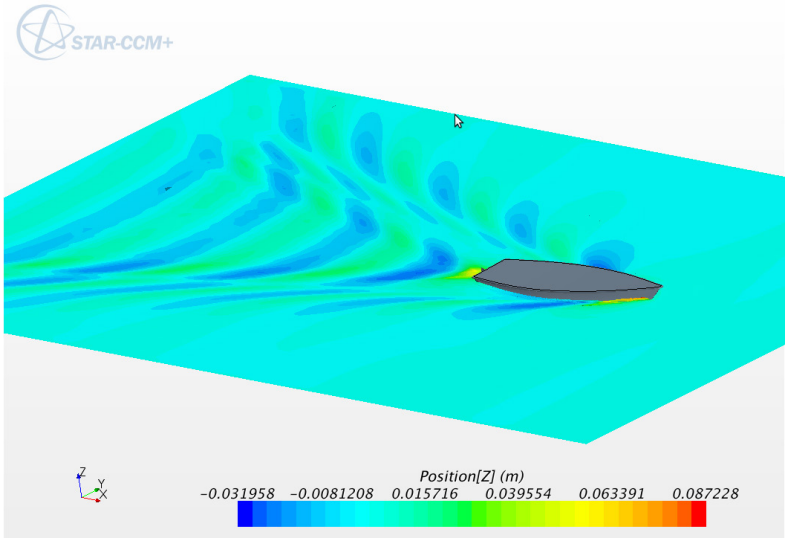

Figure 15 Wave pattern withi the computational domain in 4kn

Figure 15 shows illustrates the wave pattern of the Laser in 4 kn boat speed. It can be seen that the wave pattern vanishes to the edges of the computational domain and no reflections from the sides are present. This is achieved with the very large cells of the mesh at the edges of the domain.

The average flow speed close to the walls, i.e. the hull and the appendages, was estimated using a wall function. Relatively few prism layers were therefore used and a high y^+ value of approximately 30 for the cell closest to the wall. Therefore the flow within the viscous sublayer next to the hull was fully estimated with the wall function and only the flow outside this was solved with the RANS code. The final simulations had 14 prism layers on the hull, eight on the rudder and nine on the centreboard. The prism layers on the hull and centreboard can be seen in Figure 16.

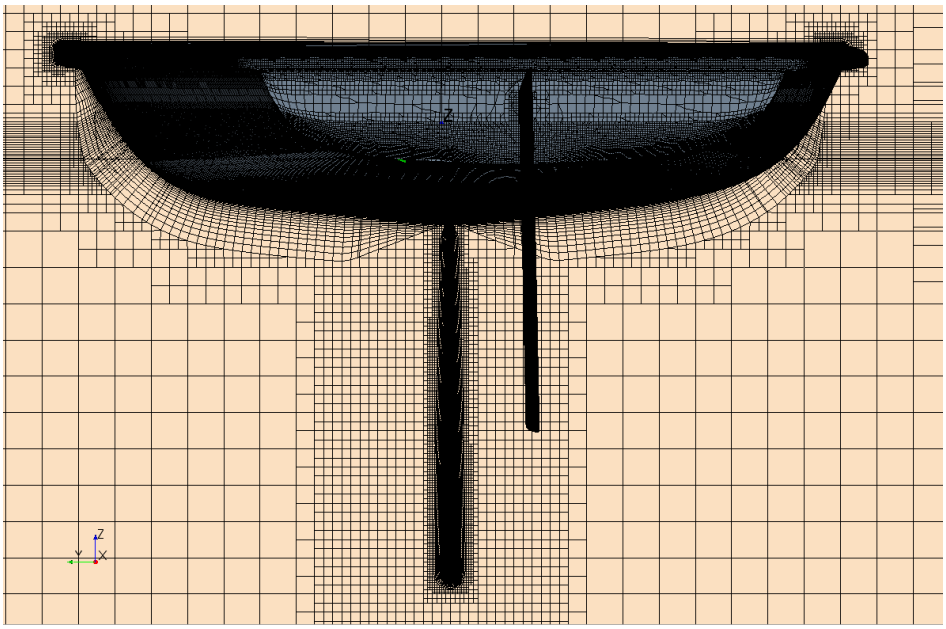

Figure 16 Aft view of the computational mesh close to the hull

The transversal plane in Figure 16 is positioned at the centreboard and shows therefore the prism layers at that transversal section but not at the rudder. The free stream flow direction is perpendicular to the transversal plane and therefore the leeway angle can also be seen well, as the centreboard and rudder are not in line.

The boundary condition used at the inlet and the sides of the domain was *velocity inlet*, meaning that a constant free stream velocity would be defined at these interfaces. The boundary condition at the outlet of the domain behind the boat was *pressure outlet*, defining the pressure, but leaving velocities to be computed from inside the computational domain. The boundary condition at all surfaces of the boat was *wall*. This means a no slip and no penetration condition. I.e. the velocity at the wall is zero and no flow can pass through the surface.

3.3 Grid Validation on Hull

A systematic study on the effects of a varying Y^+ value on the hull was made. In these simulations the appendages were not included into the model. The number of prism layers was kept constant at 14 but the Y^+ value was varied from an average of ten to an

average of 60. The results converged towards the higher Y^+ values. The results are shown and reported in detail in the results section.

3.4 Grid Validation on Appendages

A systematic mesh variation study was made to understand the effects of varying grid density, amount of prism layers and Y^+ of the first cell. The model used included the hull and both appendages.

Three different grids were created to investigate the effect of general grid density. A so called standard grid that had been used in earlier studies was used as a base case and two variations of this were created. The variations were created by shrinking the base cell size by a factor of $1/\sqrt{2}$ and $1/\sqrt[4]{2}$. The three obtained grids contained approximately seven, ten and 15 million cells.

In addition also the amount of prism layers on the appendages was varied in three steps from six to 10 cells on the rudder and from 7 to 11 cells on the centreboard. The Y^+ values of the first cell were kept constant.

A matrix of simulations was therefore created where the effect of general grid density and amount of prism layers could be evaluated. The effect of Y^+ values was not separately investigated on the foils but kept at an average of approximately 60 and at minimum values above 30.

4 Results and Discussion

This chapter will present the outcomes of the study and discuss these. It has been chosen to present and discuss the results in parallel. First, the results of the validation and verification studies related to the CFD method used will be presented and discussed. After this the results for optimal sailor position for each speed will be presented and discussed. Finally a summary is provided and the results are reflected against experiences of top level sailors.

This chapter aims to give the information on optimal sailor position and to explain and discuss the physical phenomena affecting these optimal sailor positions.

4.1 Validation

Validation is defined as a process for evaluating simulation modelling uncertainty by comparing simulation results to benchmark experimental data. When possible, validation also includes assessing the magnitude and sign of the simulation error. (Stern et al. 1999, p.2)

To validate the CFD simulations of this study, several test were made to compare simulated results with equivalent tank test cases. These tests were done without appendages as all tank tests were made without appendages. In the following two chapters validations on the accuracy of resistance prediction over the whole speed range and as a function of heel and trim are presented.

4.1.1 Upright Resistance Curve

The accuracy of the CFD computations was validated by simulating some of the cases that had been tested in the tank. Tested upright cases with the trims producing least resistance were chosen for comparison. The resistance graphs for the tank test results and the simulations are shown in Figure 17 and the amounts of error can be seen in Table 2.

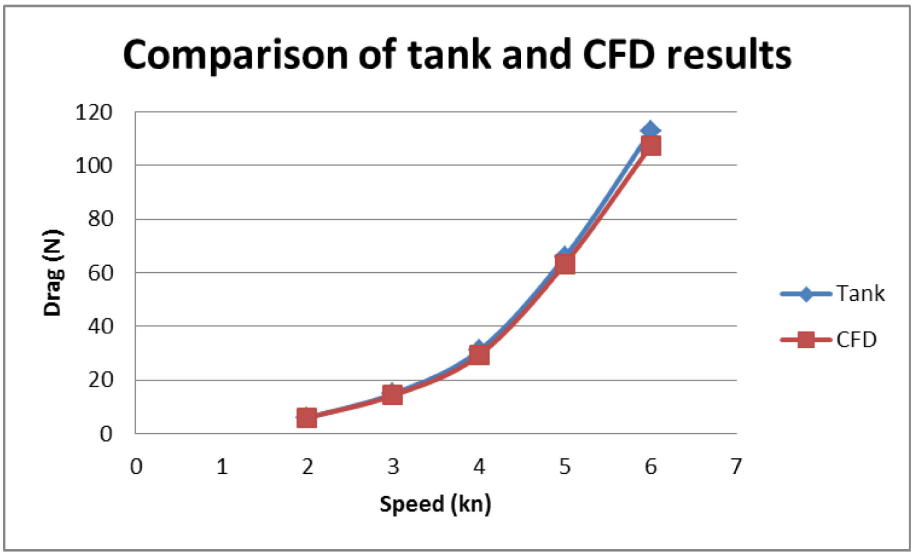

Figure 17 Comparison of upright resistances measured in tank tests and CFD simulations

Speed (kn)	Trim (deg)	Hull Upright Resistance in Tank (N)	Hull Upright Reistance in CFD (N)	Error of CFD (%)
2	-2,16	5,97	6,00	-0,5
3	-0,09	14,96	14,34	4,1
4	-0,05	31,06	29,30	5,7
5	0,5	65,93	63,36	3,9
6	1,58	112,73	107,40	4,7

Table 2 Comparison of upright resistances measured in tank tests and CFD simulations

As can be seen in Figure 2 and Table 2 the error of the CFD simulations is between 3,9 % and 5,7 % for the most relevant speed range. The simulated result is less than the result from the tank tests. At two knots of boat speed the error is only 0,5 % and the simulation is over predicting the resistance. The reason for the errors was not found within this study.

As the goal of the study was to optimize the trim and heel of the boat, the absolute values of resistance and their error have little effect on the results. However, it is important, that the trends are caught correctly, i.e. the effects of trim and heel are recognized. Therefore a few tests were made on the correlation of trimmed and heeled resistances measured in the tank and in simulations. These results are presented in the following chapter.

4.1.2 Heel and Trim

As this study concentrates on finding optimal trim and heel angles for different speeds, it is important, that the trends of increasing or decreasing resistance with changing trim or heel are recognized. Therefore a comparison between tank test results and CFD results with increasing heel was made at four knots of boat speed. The comparison was done without appendages as the tank tests were performed without them as well. Both

trim and heel were set to be equivalent in the tank and in CFD calculations for each case.

While the tank tests showed an 11 % reduction of resistance at the maximum tested heel angle, the resistance reduction in the CFD results was 8,2 %. The results are shown in Figure 18 and Table 3.

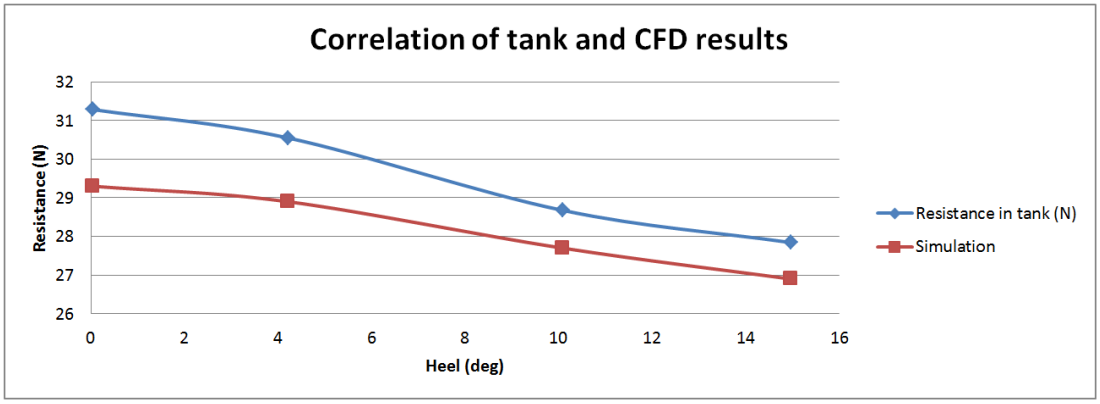

Figure 18 Correlation of resistance minima in tank tests and CFD simulations

Heel (deg)	Resistance in tank (N)	Percentage of upright resistance in tank (%)	Resistance Simulated (N)	resistance simulated (%)	Deifference of change, tank vs. simulation (%)
0,05	31,283	100,0	29,3	100,0	0,0
4,21	30,551	97,7	28,9	98,6	1,0
10,08	28,677	91,7	27,7	94,5	2,9
14,96	27,842	89,0	26,9	91,8	2,8

Table 3 Correlation of resistance minima in tank tests and CFD simulations

In the comparison of tank test results and simulations with varied trim the minimum in resistance was found at the same trim angle. The accuracy of this study is limited by the relatively coarse tank test scheme. The resistance curves as a function of trim are shown in Figure 19.

To investigate the effect of the appendages and the leeway angle also a case including appendages and a leeway angle was tested. The comparison was done with four knots of boat speed, zero heel and a five degree yaw angle. The results are shown in Figure 19. The optimal trim showed to be unchanged with the addition of appendages. It can be seen, that the minima in resistance with and without foils occur at the same trim within the accuracy of the simulations.

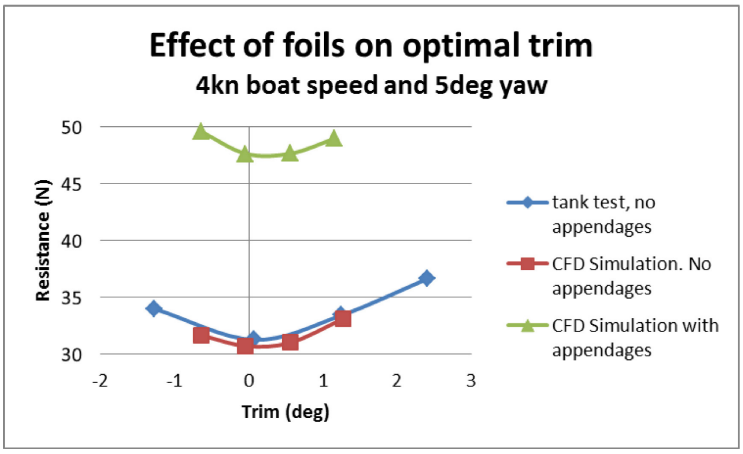

Figure 19 Comparison of resistance minima in the tank and in CFD simulations without and with foils

Figure 19 also shows the slight under prediction of resistance discussed earlier. The addition of resistance due to the appendages and a leeway angle can as well be seen in Figure 19.

4.2 Verification of the Computational Mesh

Verification is defined as a process for evaluating simulation numerical uncertainty by comparing simulation results to benchmark experimental data. When possible, validation also includes assessing the magnitude and sign of the simulation numerical error and the uncertainty in that estimate. (Stern et al. 1999, p.2)

Normally verification of numerical error would be performed before the validation against experimental benchmark data. In this study however, the mesh used for validation was based on previous verification performed within Chalmers University and therefore no verification was initially done within this thesis. During the validations some shortcomings in the previous verifications were found and therefore new verifications were made and are presented in this chapter. Finally the chosen meshes were the same as the ones used in the validations.

To make sure that a reasonable computational mesh is created and chosen, the mesh was verified by testing several versions of it. The amount of cells on a CFD mesh is critical as it has to be dense enough to capture all the flow phenomena with reasonable accuracy, but on the other hand the mesh should be as coarse as possible to reduce the computational time.

Three different grids were created to investigate the effect of general grid density. A so called standard grid that had been used in earlier studies was used as a base case and two variations of this were created. The variations were created by shrinking the base cell size by a factor of $1/\sqrt{2}$ and $1/\sqrt[4]{2}$. The three obtained grids contained approximately seven, ten and 15 million cells.

In addition also the amount of prism layers on the appendages was varied from six to 10 cells on the rudder and from seven to 11 cells on the centreboard. The Y^+ values of the first cell were kept constant. All simulations of the study were performed in four knots of boats speed, in upright condition with a five degree yaw angle.

The results of the grid density study are shown in Table 4. Both absolute values of drag and side force are shown as well as the percentage of change compared to the bolded reference grid. The three groups in vertical direction represent the different densities of the main meshes. It can be seen that the change of grid density has a small effect, but with only three grids tested, it is not possible to say whether the resistance converges when the grid gets denser. The variation of the amount of prism layers shows to have very small or no impact on the resistance values.

grid	prisms rudder	prisms CB	cells (million)	drag (N)	drag change (%)	Side Force (N)	Side Force change (%)
standard	6	7	6,99	47,9	0,00	203,6	0,10
standard	**8**	**9**	**7,09**	**47,9**	**0,00**	**203,4**	**0,00**
standard	10	11	7,21	47,9	0,00	203,6	0,10
medium	6	7	10,4	47,6	-0,63	203,2	-0,10
medium	8	9	10,56	47,7	-0,42	202,8	-0,29
medium	10	11	10,71	47,7	-0,42	202,9	-0,25
dense	8	9	15,33	47,3	-1,25	201,7	-0,84
dense	10	11	15,54	47,3	-1,25	201,8	0,79

Table 4 Grid density study

The result of the amount of prism layers having so little effect on the resistance is somewhat surprising. This underlines the dominating nature of the wall function used to solve the viscous boundary layer, and shows that few prism layers are enough within the boundary layer if the wall function is used. This also means that the flow within the boundary layer is not solved very accurately. To study the boundary layer more carefully, this method would not be suited.

To evaluate the effect of first cell Y^+-values the chosen standard grid was further refined into five more grids with constant general grid density and constant amount of prism layers but varying first cell Y^+-values. As it was unclear what the so called all Y^+ treatment in Star CCM+ does, also small Y^+-values below 30 were investigated. Clearly the results converge towards higher Y^+-values and therefore a higher Y^+ grid was chosen. The results can be seen in Table 5, Figure 20 and Figure 21. The bolded grid, which has a Y^+-value of 30 to 75 in the cells closest to the surface, is the one used in further simulations.

Change of results with varying first cell Y+ values

grid	prisms on foils	Y+	Hull drag (%)	CB drag (%)	Rudder drag (%)	Total Drag (%)	Hull SF (%)	CB SF (%)	Rudder SF (%)	Total SF (%)
standard	8/9	5-20	0,1	9,3	7,8	2,7	-4,6	4,6	11,4	4,2
standard	8/9	10-35	0,1	4,1	3,8	1,3	-5,1	3,4	9,0	3,1
standard	8/9	20-45	0,1	2,0	2,0	0,5	-5,7	2,4	7,6	1,9
standard	8/9	24-60	0,0	0,7	0,3	0,2	-0,2	1,0	0,6	0,8
standard	**8/9**	**30-75**	**0,0**	**0,0**	**0,0**	0,0	0,0	0,0	0,0	0,0
standard	8/9	36-85	-0,1	-0,2	-0,5	-0,2	-1,8	-0,8	-0,6	-0,9

Table 5 Y+ variation results

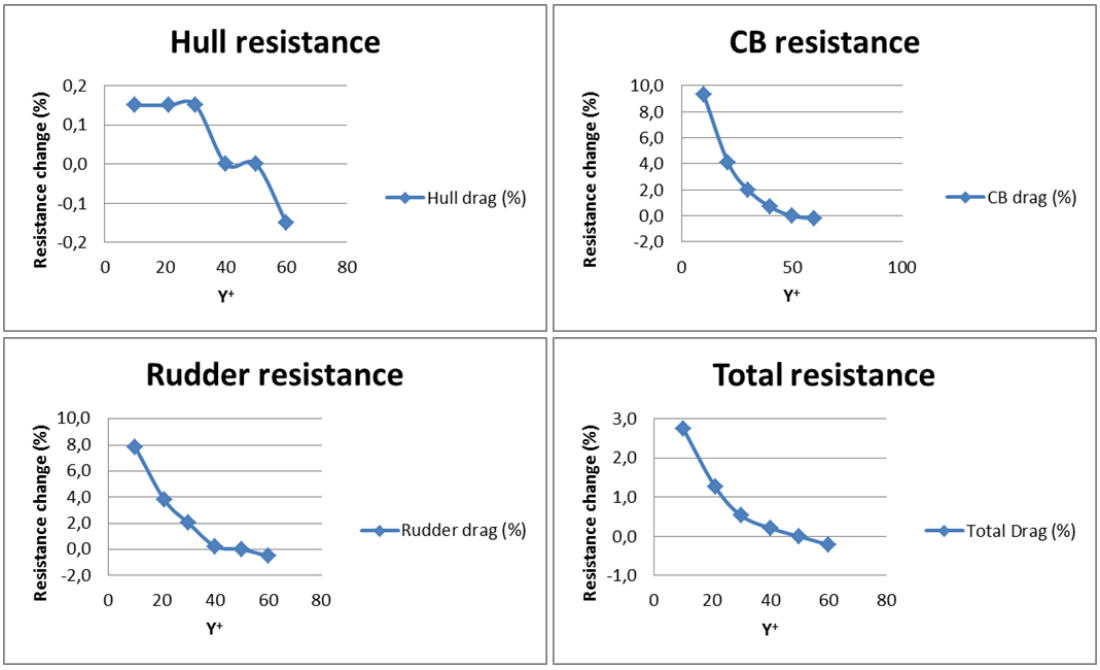

Figure 20 Resistance components as a function of Y+ variation

In Figure 20 the resistance results are shown as functions of the Y^+-value of the simulation. The results are shown for the hull, rudder and centreboard separately also for the total resistance. It can be seen that the resistances of the appendages have a tendency towards convergence, but the hull does not. Looking at the total resistance, being a sum of the components it has a tendency towards convergence, but it does not really converge yet.

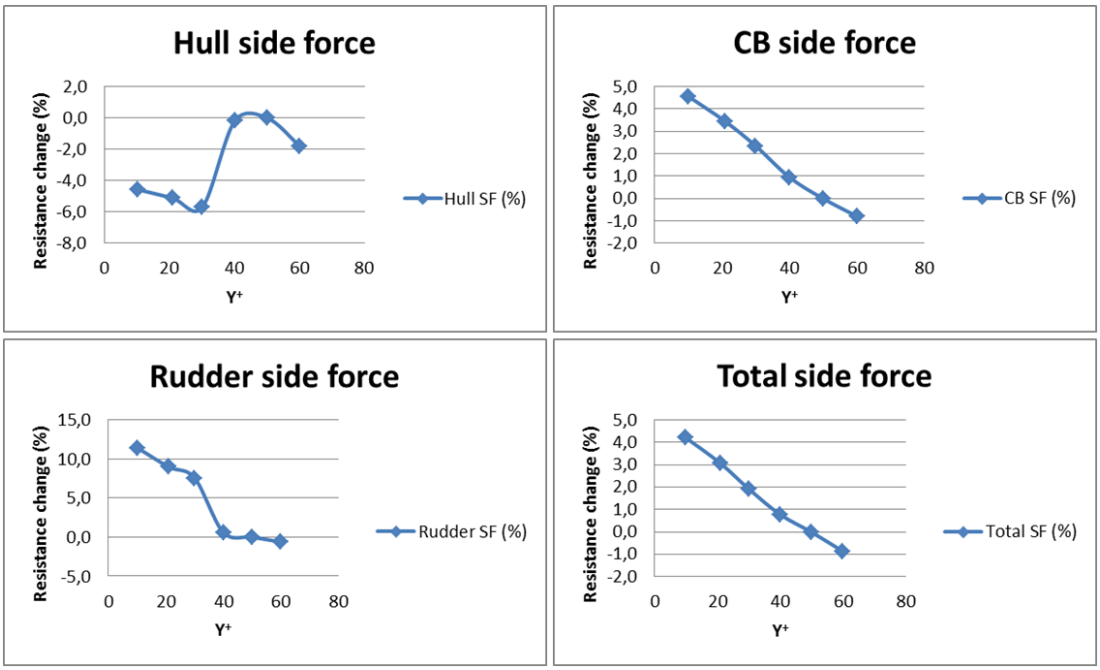

Figure 21 Side force components as a function of Y+ variation

Similarly to Figure 20, Figure 21 the side force results are shown as functions of the Y^+-value of the simulation for each component and for the whole boat. No convergence is found within the tested range of Y^+-values. The dominating component affecting also the total side force is the centreboard, and it can be seen that the graph on the total side force therefore looks very similar to the graph on the side force of the centreboard.

As proper convergence on resistance and side force was not found, the simulations cannot be regarded fully verified. Regarding the resistance the convergence is decent, but the side force did not converge. The error caused is assumed systematic and will occur in all simulations. It could therefore change the yaw angle of a result slightly, but the effect on resistance, speed or needed wind would be negligible.

4.3 Results of Simulations and Calculations on Sailor Position

The matrix of CFD calculations covered five speeds, 2, 3, 4, 5 and 5,4 knots. For each speed a series of three different heel angles were tested and for each heel angle four or five trim angles were tested. The yaw angles were constant for each speed. The highest speed of 5,4 knots was in final IVPP calculations not achieved, i.e. the top speed lies somewhere between 5 and 5,4 knots. Results are presented up to 5 knots.

For each speed, optimal trim as a function of heel is shown. This result is based on the CFD simulations performed including appendages and a constant yaw angle for each speed. The optimal trim is found at the point where the resistance is lowest. This is not an obvious result, as also the side force produced changes with trim. However, an IVPP-

analysis of different resistance and force combinations showed the optimal trim to be where the smallest resistance occurs.

Next, a plot of the drive force and the resistance as a function of heel is shown. In this graph the wind is constant for the drive force and the yaw angle is constant for the resistance. The drive force is calculated based on Hazen´s aerodynamic model and the resistance is based on the CFD simulations performed. Therefore the graphs only show the approximate characteristics of the drive force and resistance change as a function of heel. However it gives a good indication on how the forces change due to heel.

In principle, the graph demonstrates the reduction of drive force of the sail due to heel and the change of resistance due to heel. If there would be no other changing factors than heel, the ideal heel angle would always be found where the difference of the drive force and the resistance is largest. The ideal heel would then mean the highest possible speed for the given wind.

The problem of the comparison of drive force to resistance as functions of heel is that it is impossible to keep the same factors constant for both drive force and resistance. It would be fair to have either constant wind or speed on both graphs. The current graph on drive force assumes constant wind. However, for the resistance to correlate to constant wind the speed should change. Firstly this would require interpolation between the speeds investigated in CFD calculations, and secondly we would be solving the force equilibrium then already. Therefore we could not look for the largest difference of drive force and resistance anymore.

The most tempting refinement to the comparison of drive force to resistance would be to add the correction of yaw angle and therefore induced drag to the resistance curve. However, to add the correction of yaw and induced resistance the correct sail force would have to be taken into account which would require the change of wind. This again is not acceptable as this would start the loop of solving the whole equilibrium and the curves would show no difference anymore.

If more factors are taken into account in the drive force and resistance curves we enter the process of VPP calculation. This would then resemble the reality where the drive force and the resistance are always the same for a given speed, so that the force balance is achieved.

Finally, a graph for needed wind as function on heel is shown for each speed. The graph is based on the IVPP results for each heel. The point of the least needed wind indicates the most efficient sailing condition, i.e. heel angle and the corresponding trim angle.

Generally the point of the least needed wind should correlate with the biggest difference of drive force and resistance.

4.3.1 Optimal Trim and Heel in Two Knots

The tank test performed on the Laser dinghy showed a very clear tendency for the resistance to reduce with increasing forward trim. No minimum for resistance was found in the tank tests despite of large forward trim angles. However, the Laser class rules define that no body part shall be in front of the mast during racing and therefore the maximum possible forward trim in practice is much smaller than the extreme values in the tank tests. The results of the tank tests are shown in Figure 22.

The maximum forward trim in practice was estimated to be around 2 degrees. Therefore all further analysis for two knots boat speed was done for a constant trim of 2degrees forward. As the tendency of decreasing resistance with increased forward trim in tank tests was that clear, an exception for this speed was made and no trims were investigated including appendages by means of CFD simulations. Also, as the speed is low and wave making very small in this speed, it seems very unlikely that the tendency of decreasing resistance with increasing forward trim would change with the addition of appendages. Possible reasons for this tendency to change would be a wave rising in the area of the centreboard with increased heel or the change of the pressure field around the hull and therefore adding resistance. However, both cases are very unlikely as the dominant resistance component is frictional resistance. (Molland et al. 2011,p.12-16)

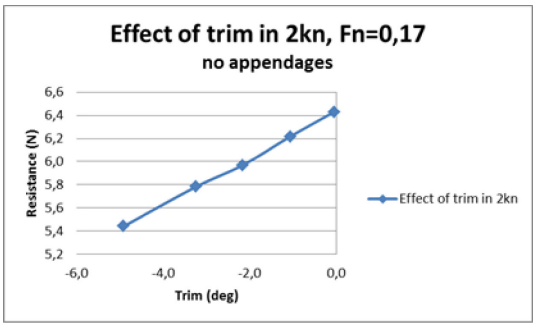

Figure 22 Tank test results on resistance change due to trim

The graph on drive force in Figure 23 shows a smooth decrease as the only factor in this analysis affecting the force is the geometric correlation, i.e. the change of the projected area to the wind and the effective angles of attack. The graph on resistance in Figure 23 shows a small hump at small heel angles and then decreases smoothly. The largest difference of drive force and resistance can be see somewhere between ten and fifteen degrees of heel. This also correlates with the graph of needed true wind in Figure 23 where the smallest needed wind occurs just above ten degrees of heel.

It can be observed that the resistance curve in Figure 23 slightly differs in shape from the one shown as a characteristic picture in Figure 3**Error! Reference source not found.**. The graph in Figure 3**Error! Reference source not found.** is based on tank test results in four knots and therefore does not include appendages. The smooth reduction

of resistance in tank tests will mainly be due to the decrease of wetted surface area (ITTC 2000). Some effects on wave resistance might be present as well, but as the displacement is constant and speed does not change no significant reduction in wave resistance can be expected (Irens 2004). Also the underwater body gets highly unsymmetrical as the boat heels, which could add the wave resistance (Claughton et al. 2012).

It seems therefore likely, that the hump on the resistance curve in Figure 23 is caused by the appendages. To fully determine the reason further investigation would be needed, but a likely reason would be the rise of surface wave when the centreboard approaches the free water surface. (Hochkirch et al. 2007) It is interesting that this would occur at such low speeds, as the Froude number is only 0,17 at the speed of two knots. However, if the centreboard approaches the free water surface it could be discussed if the Froude number for the centreboard should be taken based on the chord length of the appendage. This would mean a Froude number of 0,55 for the centreboard which makes it very logical that a the centreboard would create a significant wave drag when approaching or piercing the free water surface.

Finally, in the IVPP results in Figure 23 a clear minimum of needed wind can be found at a heel angle just above 10 degrees. Even if the minimum is clear the difference between the upright wind and the wind at 10 degrees heel is only 0,9 %. A VPP analysis assuming the resistance curve to be linear between even knots shows this to correspond to a speed change of 0,013 kn which would correspond to approximately 12 meters per nautical mile sailed distance. The assumption of linear changes of resistance between even knots is of course crude, but as changes are small this serves well as an estimate to give an idea on how large the differences are when sailing. The distance of 12 meters per nautical mile is small but significant. It might be a difference that is hard to find with traditional speed tuning, but if a sailor is confident on the sailing technique he could gain an advantage with this (Frost et al. 1991).

The optimal longitudinal position for the sailor is as far forward as possible. To achieve the two degree forward trim used in this study, the sailor´s centre of gravity has to be at 241 cm measured from the transom. The optimal transverse position for the sailor is at 20 cm leeward from the centreline. The target heel is approximately 11 degrees. The target trim is as far forward as possible.

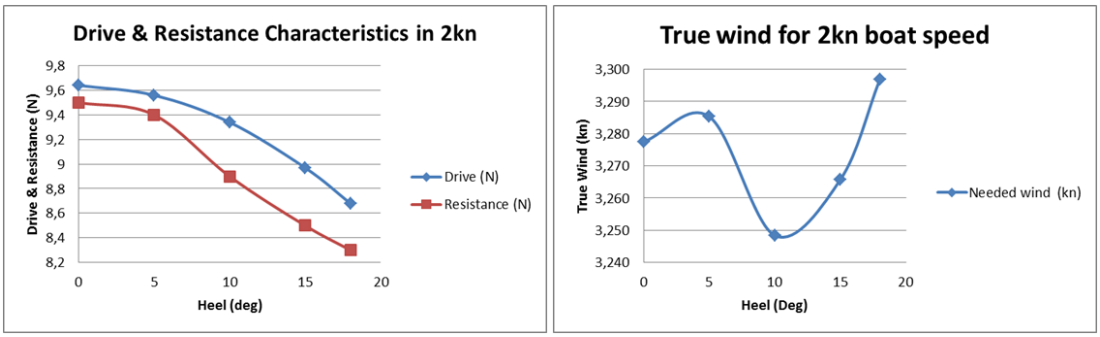

Figure 23 2kn - Drive force and resistance characteristics | IVPP results for least needed wind

4.3.2 Optimal Trim and Heel in Three Knots

In three knots boat speed the matrix of CFD simulations comprised the heel angles zero, eight and sixteen degrees. For each heel angle again, five different trim angles were investigated. In Figure 24 the results for the resistance change as a function of heel at each heel angle are shown. Finally a graph on the optimum trim as a function of heel is shown.

It can clearly be seen that the optimum trim moves further forward as the boat heels and at zero degrees heel the optimal trim is approximately 0,25 degrees aft whereas the optimal trim for a sixteen degree heel angle is approximately -0,5 degrees forward. This resembles the natural trim behaviour of the boat as it heels, i.e. as the boat is of relatively triangular shape the transom rises compared to the bow with increased heel if the centre of gravity is not moved in longitudinal direction. Also the transom immersion is a significant factor affecting the resistance (Allroth et al. 2015, Eslamdoost 2015, Orych et al. 2015). With the forward trim increasing as a function of heel, the transom immersion will stay approximately constant.

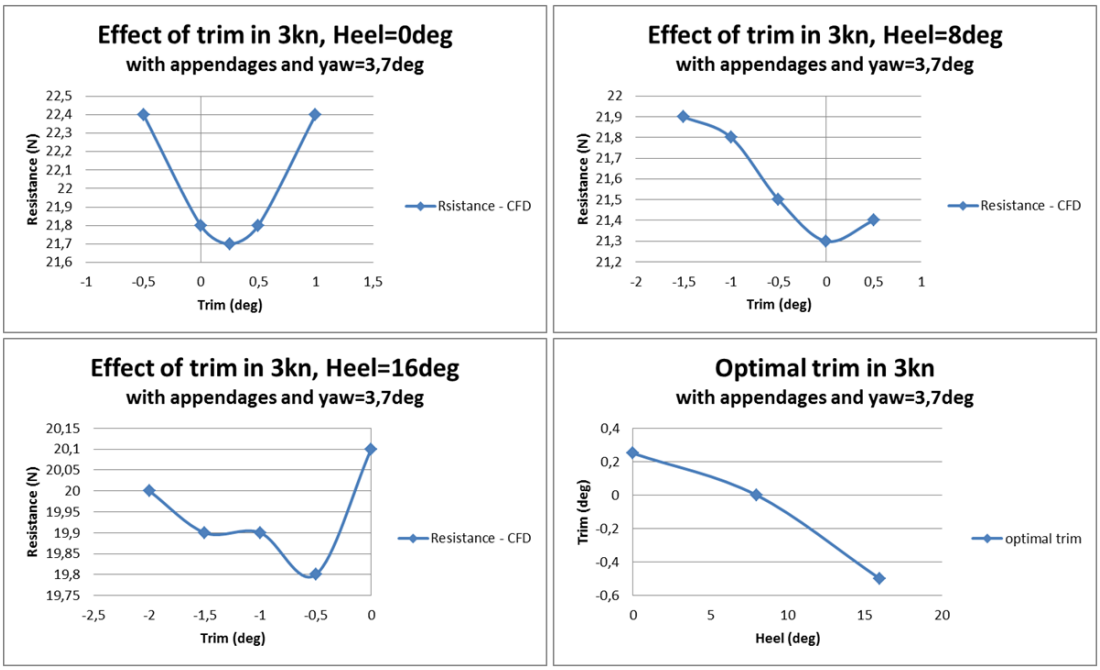

Figure 24 Optimal trims for different heel angles solved in CFD simulations in 3 kn boat speed

In Figure 25 the drive force and resistance characteristics are shown for three knots. As discussed earlier, the aerodynamic force is shown for constant wind whereas the resistance is shown for constant boat speed and with a constant yaw angle. Therefore the graphs solely show the characteristics of the change of the forces as a function of heel. The graphs now resemble less control points than in two knot boat speed and therefore the possible hump in the resistance curve is impossible to identify. The smaller amount of control points is due to fewer CFD simulated heel angles for other speeds than two knots.

The largest difference between the drive force and resistance is now found at a heel angle of zero degrees. This corresponds with the IVPP result in Figure 25 as the smallest needed wind to achieve the speed of three knots is found at a heel angle of 0 degrees. However, besides the optimum heel angle of zero degrees the preliminary comparison of drive force to resistance does not really correlate with the IVPP results and therefore demonstrates the need of solving the sailing equilibrium fully.

The factors not taken into account in the comparison of drive force and resistance are the exact correct induced resistance and the change of required wind speed as a function of heel. In this case the constant yaw angle of the CFD simulations was very closely correct for the upright condition, but too small for the heeled conditions. Therefore the induced drag in the resistance graph of Figure 25 is too small at large heel angles. In this case however, the drive force would also be increased at large heel angles if the increase of required wind would be taken into account. However, as can be seen in the IVPP results of Figure 25 the effect of increased induced resistance is dominating the end result with a linear correlation of needed wind to heel angle. The linearity should

not be taken as an exact result, as the accuracy of the result is limited by the amount of CFD simulated cases.

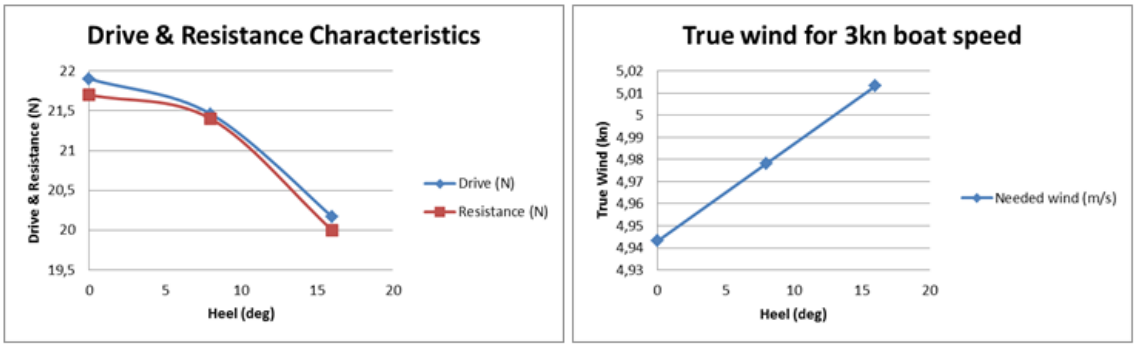

Figure 25 3kn - Drive force and resistance characteristics | IVPP results for least needed wind

Finally, the smallest required wind to achieve three knots boat speed is found at the upright condition. The result looks clear, but the change of wind from zero to eight degrees heel is only 0,018 m/s which corresponds to a wind change of 0,7 %. This is a very small difference in wind that could not even be felt by a professional sailor. However, a VPP analysis based on the same principles as the IVPP in this study shows that the wind difference corresponds to a speed difference of approximately 0,065 kn which equals 40 m/nm. This difference is significant and can be recognized by a high level sailor fairly easily.

The optimal longitudinal position for the sailor (centre of gravity) is at 165 cm measured from the transom. The optimal transverse position for the sailor is at 31 cm from the centreline. The target heel is zero degrees and the target trim is 0,25 degrees aft.

4.3.3 Optimal Trim and Heel in Four Knots

In four knots boat speed the matrix of CFD simulations comprised the heel angles zero, seven and fourteen degrees. For each heel angle again, four or five different trim angles were investigated. In Figure 26 the results for the resistance change as a function of heel at each heel angle are shown. Finally a graph on the optimum trim as a function of heel is shown.

In very similar manner to the results in three knots boat speed it can clearly be seen that the optimum trim moves further forward as the boat heels. At zero degrees heel the optimal trim is approximately 0,25 degrees aft whereas the optimal trim for a sixteen degree heel angle is approximately -0,25 degrees forward. As discussed in the case of three knots boat speed this resembles the natural trim behaviour of the boat as it heels. With the forward trim increasing as a function of heel, the transom immersion will stay approximately constant.

As can be seen in Figure 26 in the graph on optimal trim the optimal trim shows to have a linear correlation to the heel angle. The linearity however, has to be taken as an approximate result as the accuracy of the study is limited by the amount of CFD simulations. Comparing the results of three and four knots boat speed the correlation of optimal trim with changing heel shows a linear result for four knots but for three knots not. Looking at the control points, i.e. the simulated CFD cases the four knots case has one more control point at large heel angles than the case of three knots. The difference of the shape of the graph on optimal trim versus heel might be due to this difference. As mentioned, the linearity should therefore not be literally but rather only the trend of added forward trim with increasing heel should be looked at.

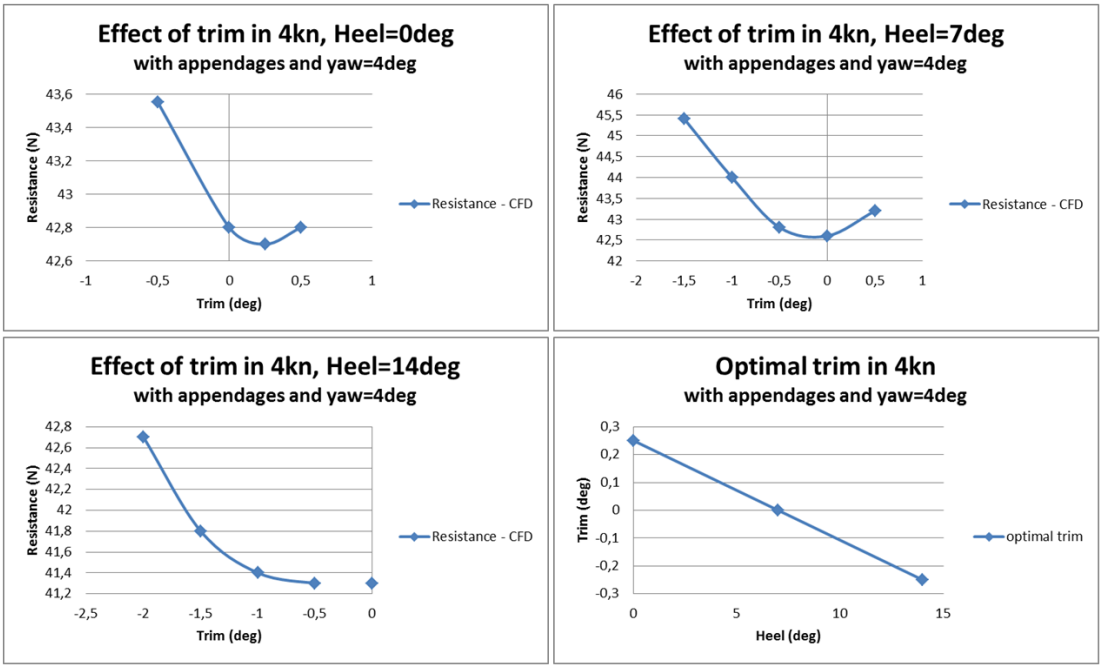

Figure 26 4kn - Optimal trims for different heel angles solved in CFD simulations

In Figure 27 the drive force and resistance characteristics are shown for four knots. As discussed earlier both graphs have their limitations as it is impossible have the same conditions for both drive force and resistance without solving the full force balance. If the full force balance again is solved, the graphs equal each other and no difference or optimal point of heel can be found with this technique.

In the case of four knots boat speed however, it is very clear that the largest drive force compared to resistance occurs at the upright condition as can be seen in Figure 27. The sail force decreases with increased heel due to the geometric correlation of lost projected area. The resistance however, differing from the cases in two and three knots boat speed, now first increases with added heel. Comparing this with Figure 3 where the resistance of the bare hull as a function of heel was shown for a boat speed of four

knots, we can see that the resistance trend has completely changed with the addition of a yaw angle. The likely reason for this is the rise of a surface wave from the centre board when the centreboard approaches the free water surface with increasing heel. Also a similar effect might occur at the rudder. However, this is questionable as the rudder is exposed to the free water surface at all heel angles.

Finally, the IVPP results for four knots boat speed are shown in Figure 27. It can be seen that the result is very similar to the result in three knots and shows a clear minimum of needed wind speed at zero degrees of heel. Also here the linearity of the curve on needed wind for three knots boat speed in Figure 25 compared to the slight nonlinearity in the corresponding curve in Figure 27 should only be taken as approximate due to a limited. However, as the control points are based on CFD simulations that have only small correction to induced drag and no interpolation between the simulated results has been made the data is very accurate.

The uncertainty comes from the limited amount of cases simulated with different trim. Therefore it is guaranteed that the absolute minimum in resistance is found for each heel which would affect the IVPP results slightly. This error would however be very small which can be seen in the graphs in Figure 26. The resistance curves follow smooth paths and it can be expected that no significantly lower points could be found.

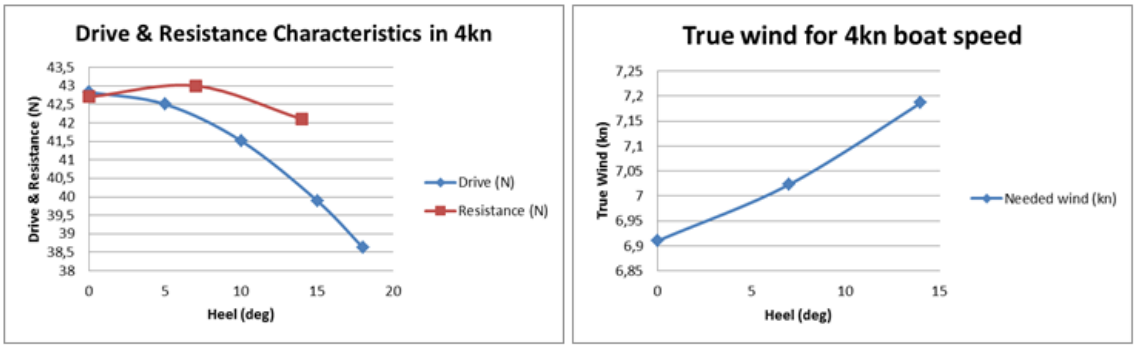

Figure 27 4kn - Drive force and resistance characteristics | IVPP results for least needed wind

In the case of 4 knots boat speed the result on the upright condition being the most favourable is clear. The difference in needed wind speed in zero and seven degrees of heel is 0,11 kn or 1,63 %. A VPP analysis based on the same principles as the IVPP in this study but in addition assuming linear change of resistance between the investigated speeds, shows that this wind change corresponds to a speed change of approximately 0,24 kn being 5,9 %. Per nautical mile this means 110 m/nm and is therefore very significant. This is a difference that can be easily recognized my most sailors within speed testing.

The optimal longitudinal position for the sailor (centre of gravity) is at 161 cm measured from the transom. The optimal transverse position for the sailor is at 59 cm

from the centreline. The target heel is zero degrees and the target trim is 0,25 degrees aft.

4.3.4 Optimal Trim and Heel in Five Knots

In five knots boat speed the matrix of CFD simulations comprised the heel angles zero, five and 10 degrees. For each heel angle again, four different trim angles were investigated. In Figure 28 the results for the resistance change as a function of heel at each heel angle are shown. Finally a graph on the optimum trim as a function of heel is shown.

In very similar manner to the results in three and four knots of boat speed it can clearly be seen that the optimum trim moves further forward as the boat heels. At zero degrees heel the optimal trim is approximately 0,25 degrees aft whereas the optimal trim for a ten degree heel angle is approximately -0,25 degrees forward. As discussed in the case of three and four knots of boat speed this resembles the natural trim behaviour of the boat as it heels. With the forward trim increasing as a function of heel, the transom immersion will stay approximately constant.

As can be seen in Figure 28 in the graph on optimal trim the optimal trim shows to have a linear correlation to the heel angle. The matter of the accuracy of the results and the linearity of the optimal trim in correlation to heel has been discussed in the cases of three and four knots boat speed. The same discussion applies to the boat speed of five knots and the linearity of the graph on optimal trim as a function of heel should be taken as an approximate result.

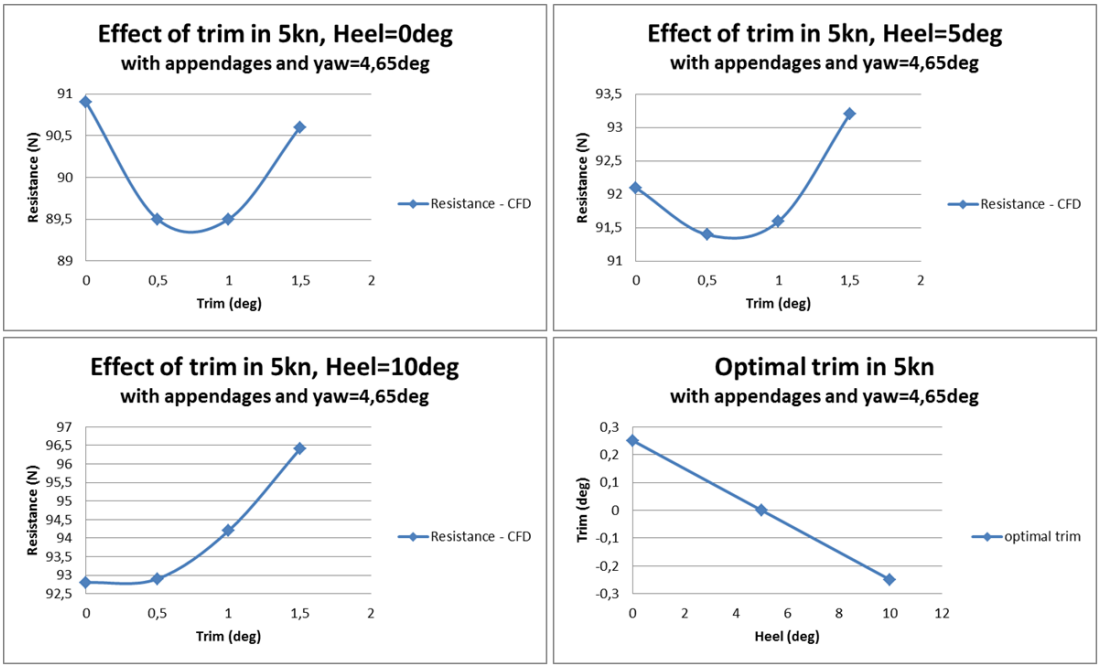

Figure 28 5kn - Optimal trims for different heel angles solved in CFD simulations

In Figure 29 the drive force and resistance characteristics are shown for five knots boat speed. Both the drive force and the resistance now change in very different manner compared to the previously discussed boat speeds. The drive force now increases dramatically with increasing heel instead of decreasing as in earlier discussed boat speed. This is due to the flattening factor that had to be utilized at the boat speed of 5 kn and at lower speeds not.

The reason for this was that at five knots boat speed the righting moment is was not sufficient to keep the boat at the desired heel angle without flattening the sail. Therefore in the graph on drive force in Figure 29 the real flattening factor for each sailing condition was used. I.e. the flattening factor is smallest at small heel angles and can be increased with larger heel angles as the righting moment increases due to the centre of buoyancy moving further away from the boat´s centre line. The flattening factor for each heel angle is shown in Figure 30. The flattening factor is always the largest possible for each angle, i.e. the least possible amount of flattening is used for each heel angle.

The resistance graph in Figure 29 shows a very linear correlation of Resistance to heel. Also, it can be seen that the change of resistance as a function of heel is relatively small. The linearity and small change is perhaps a little surprising as when compared to lower speeds. However, the Froude number is relatively high for a sailboat at Fn=0,43 dynamic lift on the hull start to play a role. Regarding dynamic lift the upright condition would most likely be most favourable. However other effects like the increasing wave drag and rising keel wave will have significant effects as well less present in previously discussed speeds. To address the reasoning for the linear and slightly increasing resistance the hydrodynamics around the hull and appendages would have to be studied further.

The largest difference between the drive force and the resistance with constant wind for the drive force and constant yaw angle for the resistance occurs around eight degrees of heel. In the IVPP in Figure 29 it can be seen that the least needed wind for five knots of boat speed occurs at approximately 7,5 degrees, corresponding very well to the result of the comparison of drive force and resistance.

The result of a relatively large needed heel is interesting and not necessary obvious to a sailor. In practice this means, that sailing with some heel and a fuller sail is beneficial compared to sailing the boat fully upright with a flatter sail. The dominant effect that makes the heeled condition faster is the addition of righting with heel. Therefore the sail can be significantly more powerful and a larger drive force is created.

The GZ-curve, i.e. the righting arm curve of the boat without a sailor is shown in Figure 31. The graph shows the horizontal distance from the centre of buoyancy to the centre of gravity of the boat. Firstly this distance is the righting arm of the boat itself, but also it is the added part of the righting arm for the sailors weight when the boat heels. When the boat heels the centre of buoyancy moves sideways and affects the righting moments

very significantly. The maximal estimated righting moments of the Laser with a fully hiking sailor are shown in Figure 31. It can be seen that a very significant increase in righting moment occurs already with a few degrees of heel and that the slope of the curve is steep especially at small heel angles. This growing righting moment allows for the huge gain in sail power presented in Figure 29 and includes only a small penalty in resistance.

The optimal longitudinal position for the sailor (centre of gravity) is at 166 cm measured from the transom. The optimal transverse position for the sailor is as far out as possible. The furthest out sailor position (centre of gravity) in this study was taken as 95 cm from the centreline. The target heel is around 7,5 degrees. The target trim is 0,25 degrees aft.

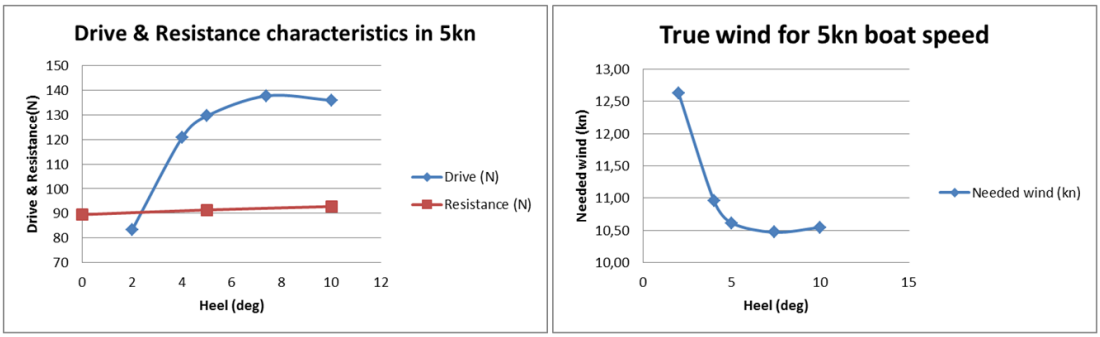

Figure 29 5kn - Drive force and resistance characteristics | IVPP results for least needed wind

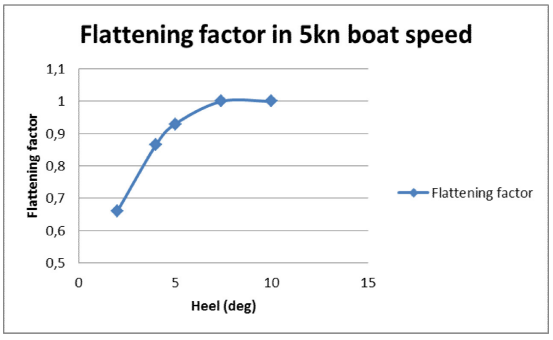

Figure 30 5kn - flattening factor for different heel angles

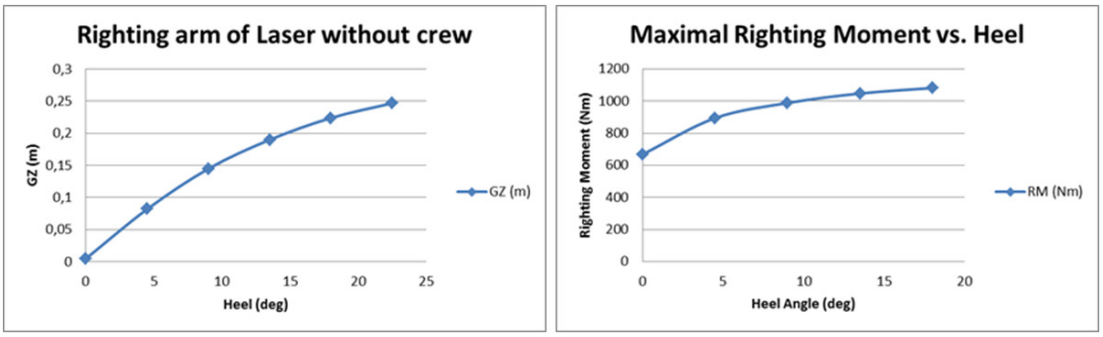

Figure 31 Righting arm of the Laser | Maximal righting moment with a 82kg crew

4.3.5 Summary on Optimal Sailor Position

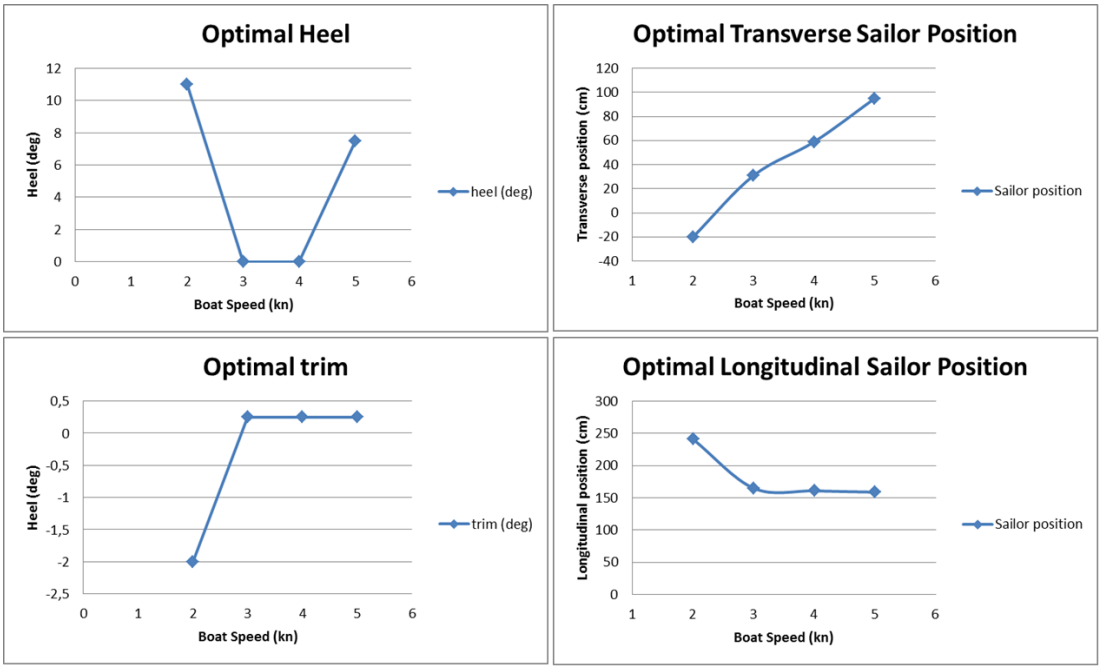

Figure 32 Summary on optimal heel and trim angles and sailor positions

Figure 32 shows a summary on optimal trims and sailor positions. It can be seen, that the ideal heel angle is first relatively large, decreases then to be completely upright at medium speeds and then again rises to a significant heel angle at higher speeds. At low speeds the reason for the heel is the reduction of wetted surface area, at medium speeds the reason for the upright condition is the added sail power, and at higher speed the reason for the growing heel angle is the added righting moment which in turn makes an increase in sail power possible. To achieve these heel angles the sailor moves transversally out in the boat with increasing speed starting on the leeward side of the centreline and ending at a fully hiking position.

The optimal trim again is as far forward as possible in low speed and at medium and higher speed the optimal trim is very constant at approximately 0,25 degrees aft. The optimal trim is achieved in low speed by moving as far forward as possible and in medium and higher speeds the optimal sailor position is around 160-166 cm from the transom with only small sailor movements.

5 Conclusions and Future Work

5.1 Finding the Optimal Sailor Position

This study investigates the optimal sailor position on a Laser dinghy sailing upwind in flat water. A large effort has been made to investigate the hydrodynamic forces through CFD simulations and significant understanding on the topic has been gained. The aerodynamic forces have been assessed only in a brief manner through Hazen´s experimental aerodynamic model (Hazen 1980). As the hydrodynamic and aerodynamic forces on a sailing yacht are highly coupled and the optimal sailing conditions were solved using the IVPP combining all the forces acting on the Laser, also inaccuracies in the aerodynamic model will have some effect on the results.

Analysing the importance of correct sail forces it becomes clear that the absolute values of the sail forces are not that critical. A small error in sail forces would make a small difference in the wind speeds at which the outlined phenomena happen, but it would not change the characteristics of heeling in very light winds, then sailing upright in light conditions and finally heeling slightly in medium and stronger conditions. A mistake however in estimating the change of sail forces due to heel could make a difference in the characteristics of the results. The effective angle theorem assuming the effective inflow in the plane perpendicular to the mast to be the only component affecting lift and drag (Kerwin 1978) has been questioned within research (Jackson 2001). Further studies have shown that that the effective angle theorem does not completely apply, however errors become significant only at larger angles of attach and larger heel angles (Fossati 2008). As this study only investigates sailing close hauled upwind and the Laser is sailed at small heel angles compared to larger yachts, the errors in the aerodynamic model due to change of heel angle will not affect the results significantly.

Based on the previous discussion the results of this study can be assumed valid. However, it is another matter to comment on sail trim, which of course is coupled with the optimal sailing trim and heel. A natural continuation on this study would be a study within the aerodynamics.

Based on discussions with Olympic Laser sailors, the results of this thesis do not conflict with practical experiences. Professional sailors normally have established techniques but research results can give sailors confidence and new ideas to test. From the sailor´s point of views key findings in this thesis are the trim and heel in very light conditions, the very small forward and aft movement of the sailor within normal upwind speeds and the significant addition of righting moment due to heel. The optimal heel in very light wind is something that is difficult to evaluate due to the speed differences being very small, and therefore an interesting result to obtain in another way. The added righting moment due to heel again is a technical detail that many sailors would not think of. In practice this is often resembled by sailors sailing with a small heel angle. However it is helpful to understand why this heel angle occurs and is important. Still,

sailors need to hike as hard as possible in higher wind speeds, but the sailor can accept adopting a small heel angle.

The unique methodology of this thesis to develop a VPP code that works inversely, i.e. the IVPP solving the needed wind speed instead of the boat speed was a successful attempt to eliminate the need to interpolate on the highly non-linear resistance curve between the speeds. However this methodology has its limitations, as the way of presenting the results as needed wind is not obvious for many sailors. From a scientific point of view there is no difference which way the results are presented and the results of this thesis can well be compared to another VPP study.

5.2 Findings within Sailing Science

Along the process of this thesis several comparisons between existing analytic methods and CFD computations were made to understand errors or to improve the methods. Finally, development of the used analytic methods proved to be too complex within the timeframe of this thesis and the efforts were restricted to understanding the phenomena.

One of the key factors within this study was the effect of heel on resistance. Originally it was assumed, that the change in resistance due to heel would not be that different with and without foils. In the lower speeds the tank tests had confirmed the resistance to decrease significantly with increasing heel as the wetted surface area on the flat bottom gets smaller. Interestingly the reduction of resistance when heeling reduces very much when taking the foils and a constant yaw angle into account. This seems to be due to the centreboard getting closer to the free water surface and its pressure field therefore creating a wave (Hochkirch et al. 2007). Further, when the whole sailing balance is analysed the leeway angle shows to grow slightly with growing heel which also increases the resistance. Further research on the surface effects of the appendages would be needed to understand the effects better.

As final hydrodynamic data used for the IVPP calculations was corrected with analytic methods, it was important to validate the methods some extent. To estimate the side force acting on a sailing boat the coupled hydrodynamics of the hull, centreboard and rudder need to be understood. Both the interaction of centreboard and hull as well as interaction of the centreboard and rudder was studied from the CFD simulations made. Interestingly, the total side force was predicted very well by the analytic method used, but the side force distribution did not correlate with the CFD results. The analytic method overestimated the side force on the rudder achieved with a certain angle and underestimated the side force acting on the hull. As the Laser has a very shallow hull compared to most of the hulls within the Delft Systematic Yacht Hull Series which is the base for the analytic method used, it is not logical that the hull side force was underestimated. Further research in this area would needed.

The rudder was held straight compared to the hull in all simulations and drag and side force values were obtained separately for both appendages and the hull. Also the flow

direction and velocity were measured at the rudder. It turned out, that the centreboard leaves a relatively narrow wake where the flow velocity is reduced around 3 % in a boat speed of 4 knots which is significantly less than 10 % typically stated in previous studies (Larsson 2014 p.118-120, Keuning et al. 2009) However, the flow was found to turn much more than previous studies have stated (Keuning et al. 2009) resulting in a lower side force produced by the rudder than predicted by previous analytic methods.

A surprising effect was caused by the narrow wake behind the centreboard where the flow is slower and turned compared to the free stream. With changing trim or heel the side force on the rudder changes radically. It seems that this effect is caused by the rudder being just on the edge of the centreboard wake, therefore small changes in the flow field positioning it either inside or outside the wake. In practice a sailor would not notice this very easily, as the sailor rather feels the pressure on the rudder than the angle. A sailor would automatically adjust the angle to constant side force, the rudder angle being smaller outside the wake and bigger inside the wake. Further research in this area however is suggested as the effect of centreboard wake on the rudder is clearly complex and also dependent on trim and heel.

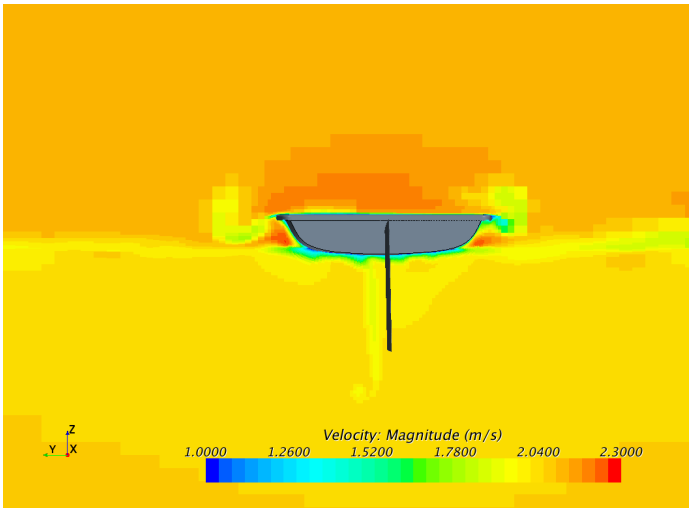

Figure 33 A section of the velocity distribution in fron of the rudder

Figure 33 shows a section of the velocity distribution in x-direction just in front of the rudder. The wake including the tip vortex of the centreboard where the flow speed is reduced can clearly be seen to the left of the rudder. In this case the wake would not interfere with the rudder or the rudder would be just at the edge of the wake and therefore experience a very small or no reduction in flow speed.

Alongside the several intriguing questions needing further research, this study has been a successful attempt to produce scientific facts around all the existing practical sailing experience. The results have shown to be in accordance with sailor experience and have also given sailors new knowledge and ideas. As a side product many interesting phenomena within sailing science have been investigated.

REFERENCES

Allroth, J, WU, T, 2014. *A CFD Investigation of Sailing Yacht Transom Sterns.* Master´s Thesis, Department of Shipping and Marine Technology, Chalmers University

Allroth, J, Wu, T, Orych, M, Larsson, L 2015. *Sailing Yacht Transom Sterns – A Systematic CFD Investigation.* 5th High Performance Sailing Yacht Conference, Auckland, March 2015.

Anderson, J, 2010. *Fundamentals of Aerodynamics.* McGraw-Hill

Axfors, B, Tunander, H 2011. *Investigation of Keel Bulbs for Sailing Yachts.* Master´s Thesis, Department of Shipping and Marine Technology, Chalmers University

Brummer, M 2013. *No Stone Unturned.* Seahorse, May 2013.

Brummer, M 2015. *Aerodynamics of the mast/Sail combination.* Finnfare, April 2015.

Böhm, C 2014. *A Velocity Prediction Procedure for Sailing Yachts with a Hydrodynamic Model Based on Fully Coupled Ranse-Free-Surface Simulations.* Doctoral thesis, University of Delft.

Campbell, J, Claughton, A 1994. *Wind Tunnel Testing of Sailing Yacht Rigs*. 13th HISWA Symposium, Amsterdam 1994.

Claughton, A, Peberton, R, Prince, M 2012. *Hull-Sailplan balance, "lead" for the 21st Century.* The International HISWA Symposium on Yacht Design and Construction 2012.

Eslamdoost, A, Larsson, L, Bensow, R 2015. *On transom clearance.* Ocean Engineering 99 (2015) 55-62.

Fossati F. 2007. *Aero-Hydrodynamics and the performance of sailing yachts* Polipress – Politecnico di Milano

Fossati, F, Muggiasca, S 2008. *Influence of Heel on Yacht Sailplan Performance.* 6th International Conference on High-Performance Marine Vehicles

Frost, R, Henderson, K 1991. *Perfectionism and reactions to athletic competition.* Journal of Sport & Exercise Psychology, Vol 13(4), Dec 1991, p. 323-335.

Gerritsma, J, Keuning J A 1985. *Model Experiments with Yacht Keels.* Seahorse Magazine, March/April1985, p. 23-26

Hazen, G S 1980. *A model of Sail Aerodynamics for diverse rig types.* New England Sailing Yacht Symposium.

Hochkirch, K, Fassardi, C 2007. *Analysis of Wave Making Resistance and Optimization of Canting Keel Bulbs.* The 18th Chesapeake Sailing Yacht Symposium, Annapolis, Maryland

Hoerner, S, 1992. *Fluid Dynamic Drag.* Published by author.

Irens, N, 2004. *The Application of Slender Hull Technology in Powered Yachts and Small Commercial Craft.* The 18th International HISWA Symposium on Yacht Design and Construction, Amsterdam 2004.

ITTC 2000. *Performance, Propulsion, 1978 Performance Prediction Method*. International Towing Tank Conference, Recommended Procedures

Jackson, P 1996. *An Improved Upwind Sail Model for VPPs.* Journal of Wind Engineering & Industrial Aerodynamics, vol. 63, 1996

Jackson, P 2001. *An improved Upwind Sail Model for VPPs.* The 15th Chesapeake Sailing Yacht Symposium, Annapolis, Maryland.

Katz, J, Plotkin, A 2001. *Low Speed Aerodynamics.* Cambridge Aerospace series.

Kervin, J 1978. *A velocity Prediction Program for Ocean racing yachts.* Report 78-11, MIT.

Keuning, J, Sonnenberg, U 1998. *Approximation of the Hydrodynamic Forces on a Sailing Yacht based on ´Delft Systematic Yacht hull Series´.* The 15th International HISWA Symposium on Yacht Design and Construction, Amsterdam.

Keuning, J, Verwerft, B, 2009. *A new Method for the Prediction of the Side Force on Keel and Rudder ofa Sailing Yacht based on the Results of the Delft Systematic Yacht Hull Series.* The 19th Chesapeake Sailing Yacht Symposium, Annapolis.

Keuning, L, 2013. *Delft Systematic Yacht Hull Series.* The 21st Chesapeake Sailing Yacht Symposium, Annapolis.

Larsson, L 1998. *Will Computational Fluid Dynamics Completely take the Role of Model Testing?* 11th WEMT International Conference, Rotterdam

Larsson, L, Raven, H, C 2010. *The Principles of Naval Architecture Series: Ship Resistance and Flow.* The Society of Naval Architects and Marine Engineers

Larsson, L, Stern, F, Visonneau, M 2013. Numerical Ship Hydrodynamics - *An assessment of the Gothenburg 2010 Workshop.*

Larsson, L, Eliasson, R.E, Orych, M 2014. *Principles of Yacht Design*. Adlard Coles Nautical

Ljungqvist, K, 2011. *Shape Optimization of an Integrated Bulb Keel.* Master´s Thesis, Department of Shipping and Marine Technology, Chalmers University

Molland, A, 2008. p.217 *Maritime Engineering Reference Book.* Butterworth Heinemann.

Molland, A, Turnock, S, Hudson, D 2011. p.12-16. *Ship Resistance and Propulsion: Practical Estimation of Propulsive Power.* Cambridge University Press

Ofshore Racing congress, 2012. *ORC VPP Documentation 2012*

Orych, M, Larsson, L 2015. *Hydrodynamic Aspects of Transom Stern Optimization.* 5th High Performance Sailing Yacht Conference, Auckland, March 2015.

Pluto, A, Konstantinos, K 2015. *A CFD Investigation of Sailing Yacht Forebodies in Head Sea.* Master´s Thesis, Department of Shipping and Marine Technology, Chalmers University

Rosen, B, Laiosa, J, Davis, W 2000. *CFD design studies for America´s Cup 2000.* American institute of Aeronautics and Astronautics

Stern, F, Wilson, R, Coleman, H, Paterson, E 1999. p.2. *Verification and Validation of CFD Results.* Iowa Institute of Hydraulic Research & Propulsion Research Center, Mechanical and Aerospace Engineering Department, University of Alabama in Huntsville

Stern, F, Yang, J, Wang, Z, Sadat-Hosseini, H, Mousaviraad, M, Bhushan, S, Xing, T 2012. *Computational Ship Hydrodynamics: Nowadays and Way Forward.* 29th Symposium on Naval Hydrodynamics

Tennekes, H, 1972. *The Logarithmic Wind Profile.* Journal of the atmospheric sciences.

Tursini, L 1953. *Leonardo Davinci and the problems of navigation and naval design.* Transactions of the Institute of Naval Architects, 95, p.97-102.

Werner, S, 2006. *Computational hydrodynamics applied to an America´s Cup class keel – best practice and validation methods.* Doctoral Thesis, Department of Shipping and Marine Technology, Chalmers University

Zou, L 2012. *CFD predictions including verification and validation of hydrodynamic forces and moments on ships in restricted waters.* Doctoral thesis, Chalmers University of Technology.